# Morphology of Polymer Blends

# 8

Toshiaki Ougizawa and Takashi Inoue

## Contents



T. Ougizawa (✉)
Department of Chemistry and Materials Science, Tokyo Institute of Technology, Meguro-ku, Tokyo, Japan
e-mail: tougizawa@op.titech.ac.jp

T. Inoue
Department of Polymer Science and Engineering, Yamagata University, Yonezawa, Japan
e-mail: tinoue@yz.yamagata-u.ac.jp

L.A. Utracki, C.A. Wilkie (eds.), *Polymer Blends Handbook*,
DOI 10.1007/978-94-007-6064-6_10,
© Springer Science+Business Media Dordrecht 2014

**Abstract**

In this chapter, as a guideline to control the phase separation morphology, the morphology formation mechanism is primarily explained. First the phase diagram and the phase separation mechanism are briefly explained to provide basic knowledge on controlling the morphology of polymer blends. Then, the effect of the shear flow on the phase diagram as a factor that influences the formation of the phase separation morphology is explained and the relation to the morphology control is shown. This is especially important in the polymer processing of polymer blends. Finally, as a control of the phase separation morphology using reactions, reaction-induced phase separation and reactive blending are explained. Because most polymer blends are immiscible, it is necessary to use some methods to obtain polymer blends that show good physical properties. Therefore, these are powerful tools for controlling the morphology in the polymer blends.

## 8.1 Introduction

It is not easy to satisfy the wide range of performance and function demanded of a material by using only one kind of polymer. Therefore, it is proper to satisfy these demands with polymer blends. Moreover, it is much easier to obtain a material that has the target characteristics by blending different polymers instead of designing and synthesizing really new polymers. Consequently, polymer blends which are composed of structurally and functionally different polymers have received much attention in terms of improving, e.g., mechanical, optical, and thermal properties, and numerous investigations have been done with these blends. However, most polymer blends are immiscible systems with dispersions of one polymer in the matrix of another, and it is not easy to improve their performance or function by simply mixing them. Hence, an effective control of the blend morphology is essential (Favis and Willis 1990; Bucknall 1977; Utracki 1982; Coran and Patel 1983).

The size level at which both polymers mix is very important, because it has a strong influence on the physical properties of the material. Whether a polymer blend that has mixed at the molecular level is better depends on its demanded performance. However, it is rare for a polymer blend to mix at a molecular level, because most polymer blends are immiscible and phase separation takes place. In addition, in the case where phase separation occurs, the physical properties greatly depend on the phase-separated morphology. Therefore, control of the phase-separated morphology is important. For example, the impact strength of polymer blends is generally controlled by the dispersed particle size, the ligament thickness, and the interfacial adhesion. If the morphology of polymer blends is altered by shear forces and the reaction during mixing, the material performance also changes. Thus, the morphology also greatly depends on how it is mixed.

In this chapter, morphology control using various mixing methods is described.

## 8.2 Phase Diagram and Phase Separation Mechanism

Generally, most polymer pairs of high molecular weight are immiscible in the range from glass transition temperature ($T_g$) to thermal decomposition temperature ($T_d$). It is difficult to mix polymers at a molecular level even for polymer pairs with similar structures, e.g., polyethylene (PE) and polypropylene (PP). To discuss the thermodynamics for the miscibility and the phase diagram of polymer blends, the Flory-Huggins equation has been widely used (Flory 1953),

$$\frac{\Delta G_M}{RT\,(V/V_r)} = \frac{\phi_1}{r_1}\ln\phi_1 + \frac{\phi_2}{r_2}\ln\phi_2 + \phi_1\phi_2\chi_{12} \tag{8.1}$$

where $\Delta G_M$ is the Gibbs free energy of mixing and $R$ is the gas constant. $V$ and $V_r$ are the total and reference volumes, respectively. The first two terms on the right-hand side of Eq. 8.1 represent the combinatorial entropy of mixing and negative value, where $\phi_i$ is the volume fraction and $r_i$ is the segment number of a polymer chain of component $i$. The third term contains the interaction parameter $\chi_{12,}$ which generally takes into account all contributions to the free energy that are not given by the combinatorial entropy. Using this Flory-Huggins equation, the miscibility of polymer blends can be described. In polymer blends, the combinatorial entropy of mixing the two polymers is a smaller negative than that of mixing two low molecular weight compounds, and the contribution to $\Delta G_M$ is very small. The miscibility tends to become better when $\Delta G_M$ decreases as $\chi_{12}$ becomes smaller. Therefore, pairs of dissimilar polymers are only miscible if there are favorable specific interactions between them leading to a negative contribution for $\Delta G_M$.

Miscible polymer blends can be classified into several categories. A blend that tends to phase-separate at low temperatures is termed an upper critical solution temperature (UCST) system, and one that separates at elevated temperatures is classified as a lower critical solution temperature (LCST) system. In addition, there are some pairs that are completely miscible and have both UCST and LCST characteristics. Figure 8.1a and b show the phase diagrams of a binary blend having LCST- and UCST-type phase behavior, respectively. The solid line is a "binodal line," which is a boundary between the one-phase and two-phase regions in the equilibrium state. The dashed line is called a "spinodal line," which satisfies the condition that the second derivative of the Gibbs free energy of mixing by composition is equal to zero ($\partial^2\Delta G/\partial\phi^2 = 0$). It is understood as a boundary that divides the style of the phase separation in a mixture, i.e., nucleation and growth (NG) type and spinodal decomposition (SD) type. The phase separation by NG takes place in the metastable region between the spinodal and the binodal lines on the phase diagram. SD occurs in the unstable region framed by the spinodal lines ($\partial^2\Delta G/\partial\phi^2 < 0$).

In NG, a small particle (nucleus) with almost equilibrium concentration from the uniform solution is generated accidentally and grows gradually with time. There is no typical periodicity in the phase-separated morphology. Some domains having different sizes and positions are observed, as shown in Fig. 8.2a. In an SD process, on the other hand, a periodic fluctuation of the concentration in the system spontaneously

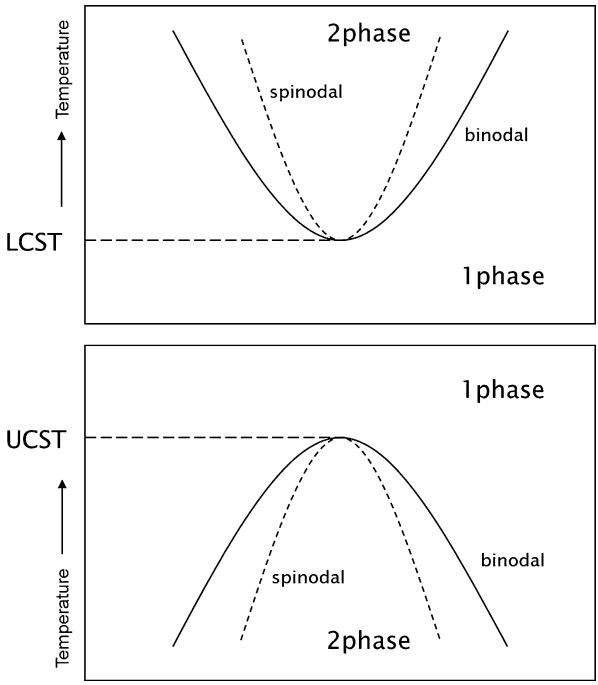


**Fig. 8.1** LCST and UCST-type phase diagrams

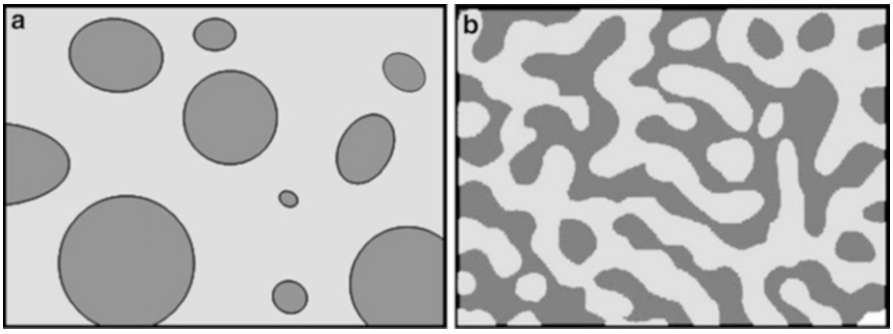


**Fig. 8.2** Schematic phase-separated morphology induced by (**a**) NG and (**b**) SD mechanism

arises. Then, the fluctuation gradually increases and separates into a coexistence composition $\phi_{B1}$ and $\phi_{B2}$. In SD, there is structural periodicity, and each phase connects mutually in three dimensions, as shown in Fig. 8.2b. Furthermore, a dissimilarity also exists in the diffusion of molecules between NG and SD. The diffusion takes place from low concentration to high concentration in the process of SD. This is the opposite direction for ordinary diffusion, which takes place in the NG mechanism (see Fig. 8.3, Cahn 1968).

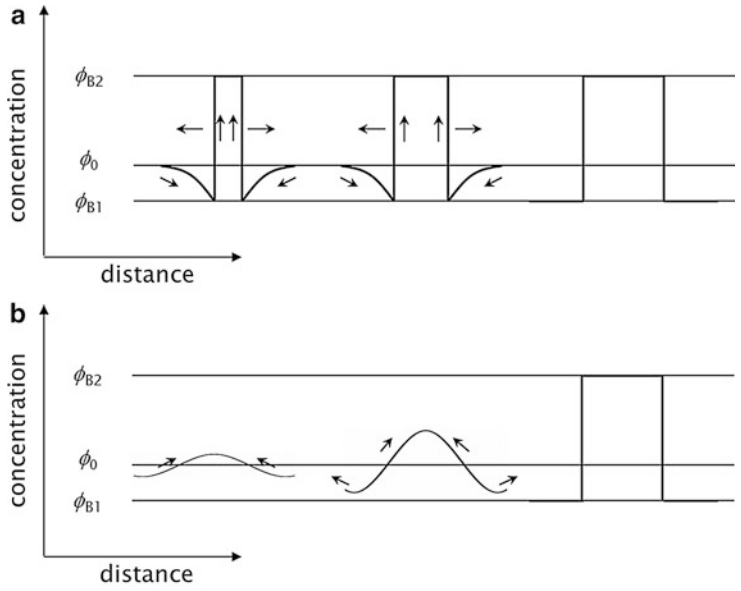


**Fig. 8.3** Growth of concentration fluctuation in (**a**) NG and (**b**) SD mechanism

SD can be divided into three stages: the initial stage, middle stage, and late stage. In the initial stage (van Aartsen 1970; Binder and Stauffer 1973), the fluctuation of the concentration is gradually generated as a monochromatic wavelength and has a constant wavelength (Cahn 1965). A co-continuous morphology having the period distance $\Lambda_m$ is formed as a consequence of the superimposed waves in various directions. The wavelength of the concentration fluctuation does not depend on time (constant), and the amplitude of the fluctuation increases exponentially. In the middle stage of SD, the periodic structure grows self-similarly, while the amplitude of the fluctuation increases gradually. In the late stage, the amplitude of the concentration fluctuation almost reaches the equilibrium concentration determined by the equilibrium composition of the blend, and then only the wavelength of the concentration fluctuation grows with self-similarity as time passes. Finally, the morphology with the dispersed particles phase (domain) in the continuous phase (matrix) is formed to reduce the interfacial tension at the late stage of SD. In this type of a system with dispersed particles, the domain size is also comparatively uniform, maintaining the regularity of the co-continuous morphology in the early stage. It can be said that the morphology after the SD is a characteristic structure.

## 8.3 Shear-Induced Phase Separation and Morphology

The effect of flow is of industrial relevance in the processing of polymer blends where high deformation rates are encountered, as in melt extrusion or injection molding.

Thus, the behavior of polymer blends in a flow field is of fundamental interest and is also technologically important, since deformation and related stresses are unavoidable in many processing steps. Recently, it has been reported that the shear flow can change the thermodynamic state of the system and perturb the phase diagram of the polymer mixtures, where it is now well established that the shear flow can shift the phase boundary a few degrees to higher or lower temperatures depending on the characterization of the blends under the shear (Mazich and Carr 1983; Lyngaae-Jorgensenn and Sondegaard 1987; Larbi et al. 1988; Katsaros et al. 1989; Nakatani et al. 1990; Kammer et al. 1991; Wu et al. 1991; Hindawi et al. 1992; Fernandez et al. 1995; Madbouly et al. 1999a). This also influences the morphologies that develop during polymer processing.

The effect of a simple shear flow on the phase behavior and morphology was investigated with the use of a parallel-plate apparatus (Fig. 8.4, Madbouly et al. 1999a) for some polymer mixtures: poly(methyl methacrylate) (PMMA)/poly(styrene-*co*-acrylonitrile) (SAN-29.5) and polystyrene (PS)/poly(vinyl methyl ether) (PVME), which have an LCST-type phase diagram; PS/PMMA, which has a UCST-type phase diagram; and polycarbonate (PC)/SAN and nylon4, 6(PA4,6)/poly(phenylene sulfide) (PPS), which are immiscible in the whole measurable region under the quiescent state.

### 8.3.1 PMMA/SAN-29.5 (AN:29.5 wt%) Mixture (LCST System)

This mixture phase-separates in the higher temperature region. Figure 8.5 shows the shear rate dependence of the cloud point at some compositions (Madbouly et al. 1999b). Since the cloud points increased monotonically for all of the measured compositions, only shear-induced mixing was observed. The shear flow can affect the phase behavior of the blend significantly; i.e., it suppresses the phase separation and enlarges the one-phase region of the polymer blend. Changes in the phase diagram of the polymer blends at different shear rates are represented in Fig. 8.6 (Madbouly et al. 1999b). The cloud points are affected by the values of the applied shear, as they gradually increase with shear rate values. Figure 8.7 represents the normalized shift in the cloud points $|\Delta T(\dot{\gamma})/T(0)| = |\{T(\dot{\gamma}) - T(0)\}/T(0)|$ versus shear rate $(\dot{\gamma})$ for different blend compositions. The following relation was given for the experimental data (Beysens and Gbadamassi 1979; Beysens and Perrot 1984):

$$|\Delta T(\dot{\gamma})/T(0)| = k\dot{\gamma}^n \tag{8.2}$$

where $k$ and $n$ are material constants that depend on composition. The experimental results can be fitted to Eq. 8.2 by using a nonlinear regression method. The constants $k$ and $n$ are used as fitting parameters. A good description of the data was obtained in Fig. 8.7, and Table 8.1 (Madbouly et al. 1999b) represents the values of the fitting parameters obtained from the regression. The values of the exponent $n$ were almost constant regardless of the composition ratio of the blend, while the values of the prefactor $k$ were greatly dependent on the composition of the

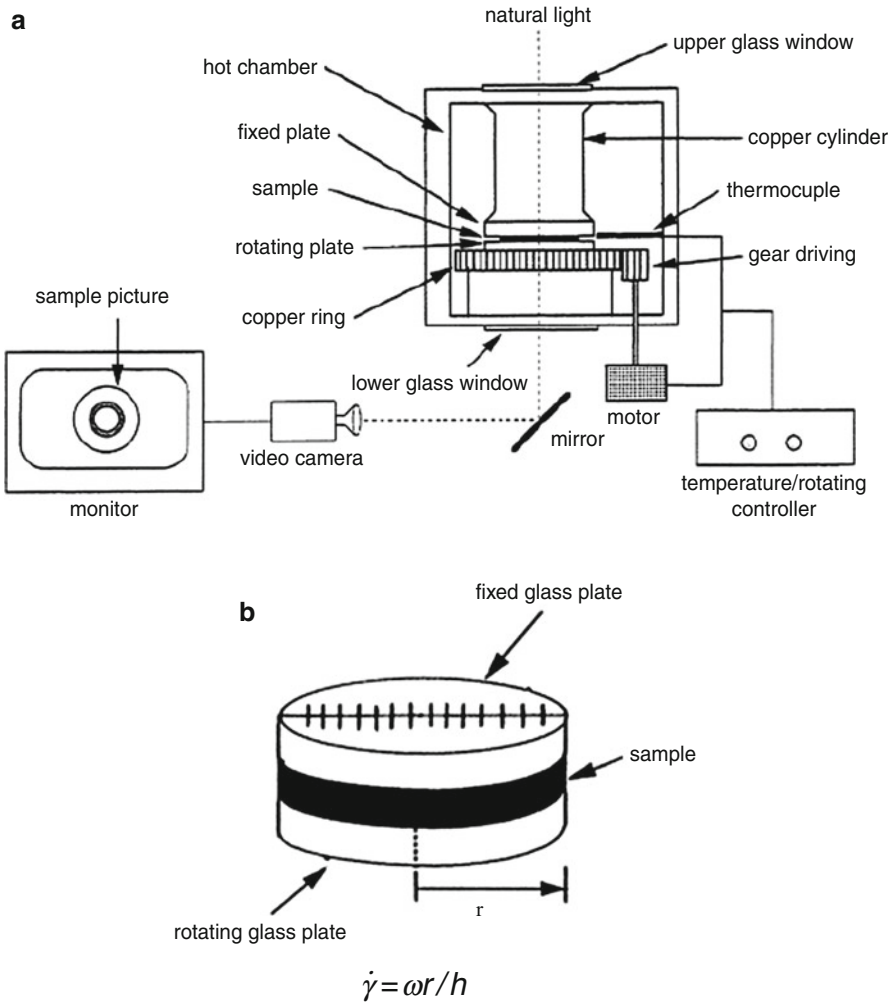


**Fig. 8.4** Schematic representation of the shear apparatus used in this work: (**a**) general drawing; (**b**) sample between two parallel glass plates

blend. The value of $k$ is a maximum for the critical composition (PMMA/SAN = 75/25) and decreases on either side of this composition. This is attributed to the critical composition being more sensitive to the shear rate effect than the other compositions, as can be seen in Figs. 8.5 and 8.6. Note that Eq. 8.2 is applicable only at small shear rate values for this system ($\dot{\gamma} \leq 12\ \mathrm{s}^{-1}$) and deviated at higher shear rates. The cloud points become almost constant at higher shear rates, as shown in Fig. 8.5.

The phase-separated morphology under a flow field has also attracted considerable attention. The morphology of this system (PMMA/SAN = 75/25) was analyzed

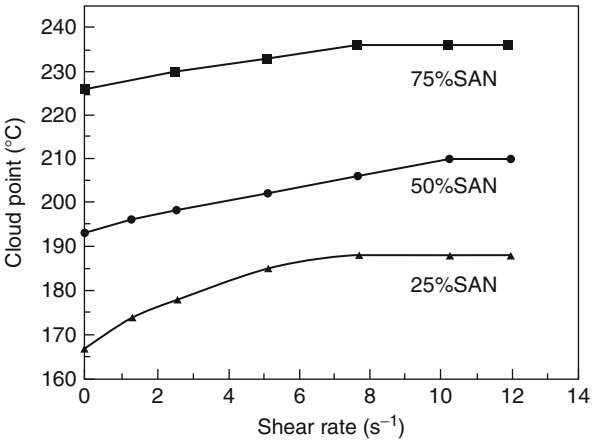


**Fig. 8.5** Shear rate dependence of cloud points in PMMA/SAN blends

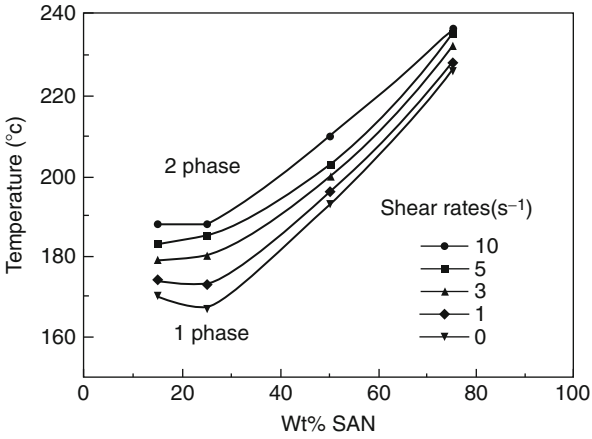


**Fig. 8.6** Phase diagrams at various shear rates of PMMA/SAN blend. Phase diagram does not change more than $\dot{\gamma} = 12\ \mathrm{s}^{-1}$

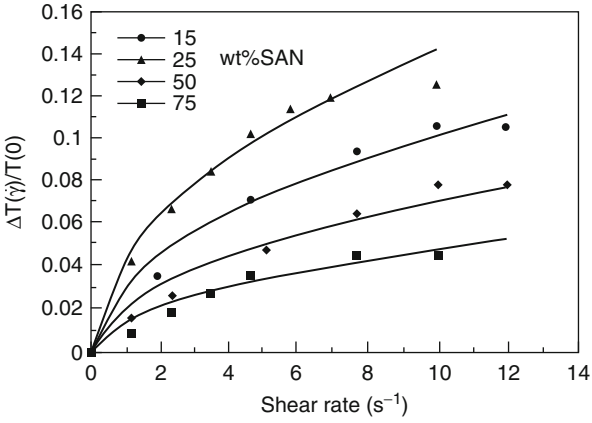


**Fig. 8.7** Normalized shift in the cloud point curve $\Delta T(\dot{\gamma})/T(0)$ as a function of $\dot{\gamma}$ for different compositions of the PMMA/SAN blends

**Table 8.1** Values of prefactor $k$ and exponent $n$ for different compositions of the PMMA/SAN blends

| PMMA wt% | $k$ | $n$ |
|---|---|---|
| 85 | 0.032 | 0.501 |
| 75 | 0.045 | 0.501 |
| 50 | 0.022 | 0.502 |
| 25 | 0.015 | 0.501 |

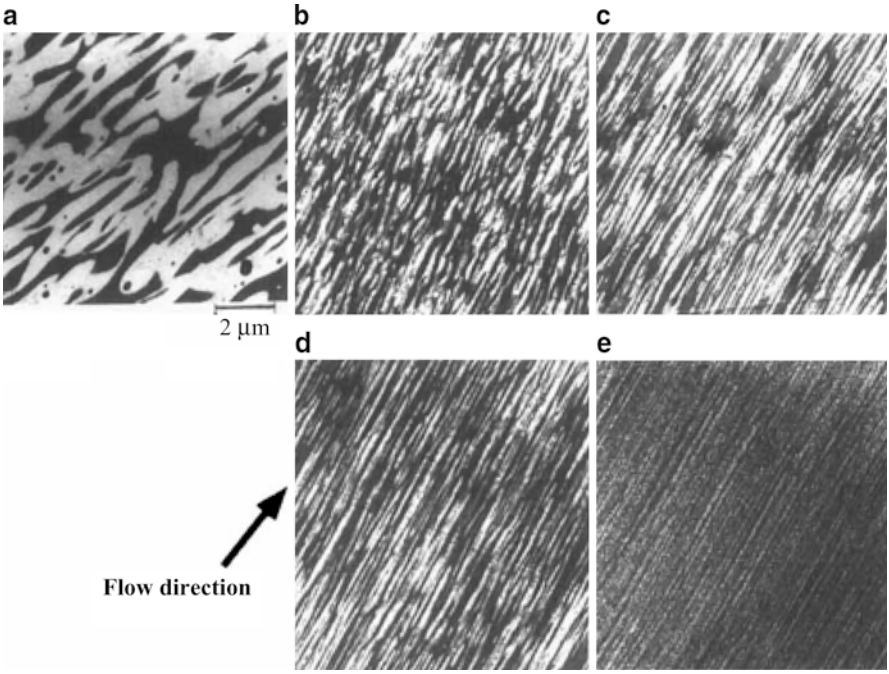


**Fig. 8.8** TEM pictures of PMMNSAN (75/25) samples that were sheared at 185 °C (20 °C above their quiescent cloud point) at 0.5 rad/s for 3 min and then quenched in a water bath. Samples were then taken from different radial positions and consequently different shear rates: (**a**) $\dot{\gamma} \sim 0\ s^{-1}$; (**b**) $1.17\ s^{-1}$; (**c**) $2.33\ s^{-1}$; (**d**) $4.7\ s^{-1}$; and (**e**) $7\ s^{-1}$

relative to the shear rate effect. The sheared sample was quickly quenched in a water bath just after the shear cessation, and the morphology was observed using a transmission electron microscope (TEM) in the sample, which was cut parallel to the flow direction. A typical observed morphology of the samples is shown in Fig. 8.8 (Madbouly et al. 1999b). The phase-separated morphology is clearly observed; the dark and bright regions correspond to SAN-rich and PMMA-rich phases, respectively. One can see a well-defined phase separation; a co-continuous two-phase morphology of the blend can be clearly observed at nearly zero shear rate. Under the shear flow, the two SAN-rich and PMMA-rich phases are elongated and highly oriented parallel to the flow direction. These TEM results indicate that the size and amplitude of the concentration fluctuations were strongly

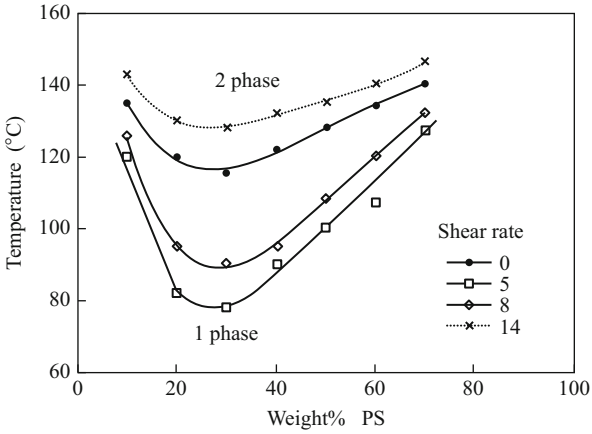


**Fig. 8.9** Phase diagrams at various shear rates of PS/PVME blend

suppressed, as indicated by the decreasing intensity and contrast of the elongated phases. Lastly, no morphology was observed, which can be attributed to the shear-induced mixing of the polymer blend at the critical shear rate value (10 $s^{-1}$). The highly oriented phases are considered to be due to the nearly equal viscosity of SAN and PMMA. According to these results, it seems that macroscopic phase separation of the polymer blends cannot occur under the steady shear flow. With increasing shear rate, the macroscopic phase boundary is broken into pieces, generating smaller domains that can be elongated in the flow direction, resulting in a decrease in contrast (i.e., decreasing concentration fluctuations). Consequently, mixing of the unlike segments is enhanced.

### 8.3.2 PS/PVME Mixture (LCST System)

Changes of the cloud points on the shear rate in the PS/PVME system are shown in Fig. 8.9, which was measured by the same method as for the PMMA/SAN system (Madbouly et al. 1999a). This phase behavior is not simpler than that of the PMMA/SAN system. At low shear rates, the cloud point curve shifts to low temperature with increasing shear rate; i.e., the two-phase region becomes larger and a maximum decrease occurs when the applied shear rate value is around 5 $s^{-1}$. Then the cloud point curve shifts to higher temperature with increasing shear rate up to $\dot{\gamma} = 14\ s^{-1}$, at which point the cloud point curve is higher than that of the quiescent state. For larger shear rates than $\dot{\gamma} = 14\ s^{-1}$, the cloud point curve does not change and becomes constant regardless of an increase in applied shear rate. This large effect of the shear rate on the miscibility behavior of this system is attributed to the large mismatch in the viscosity of the PS and PVME components: the bigger the mismatch in viscosity, the larger the effect of shear.

Based on this result, it appears that the shear flow can induce both phase demixing and mixing, as in the case of polymer solutions (Takebe et al. 1989). The fact that both were observed in the same blend suggests that two competing effects occur during

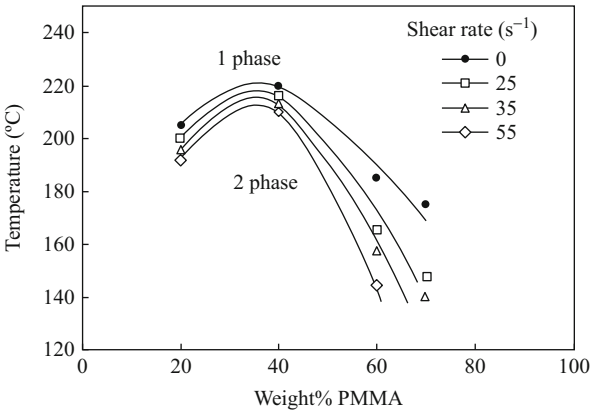


**Fig. 8.10** Phase diagrams at various shear rates of PS/PMMA blend

**Table 8.2** Values of prefactor $k$ and exponent $n$ for different systems

| System | $k$ | $n$ |
|---|---|---|
| Cyclohexane/Aniline[3,4)] | $(5.9 \pm 0.66) \times 10^{-7}$ | $0.53 \pm 0.03$ |
| Polymer solution (PS/PB/DOP)[10)] | $(2.6 \pm 0.6) \times 10^{-3}$ | $0.5 \pm 0.02$ |
| Oligomer mixture (PMMA/PS) | 0.0075 – 0.031 | $0.5 \pm 0.02$ |
| Polymer mixture (PMMA/SAN) | 0.015 – 0.045 | $0.5 \pm 0.02$ |

flow. One of these effects tends to suppress growing spatial composition fluctuation, and this effect would tend to promote phase mixing. The other effect causes the growth of composition fluctuation with consequent phase demixing. This effect can be attributed to elastic deformation, which may act to enhance some concentration fluctuation, promoting the uphill diffusion that occurs in the phase separation, as has been reported by Helfand and Fredrickson (1989) and Onuki et al. (1989). Thus, the first effect could dominate at high shear rate and high temperature, while the second effect could dominate at low shear rate and low temperature.

### 8.3.3 PS/PMMA Mixture (UCST System)

This is an oligomer mixture (Mw (PS) = 2,500, Mw (PMMA) = 6,000), and the phase separation takes place in a lower temperature region (UCST-type phase diagram; Madbouly et al. 2001). Changes in the phase diagram of the blends at different shear rates are represented in Fig. 8.10. The cloud points decreased monotonically with the shear rate. Though the results were opposite to the case of PMMA/SAN, shear-induced mixing took place. The shear effect was found to be largely composition-dependent. The shear flow can suppress the phase separation and enlarge the single-phase region of the blend.

It is important to compare the effect of the shear flow on the phase behavior for different systems. Table 8.2 summarizes the values of the prefactor ($k$) and the

exponent ($n$) in Eq. 8.2 for the four different systems. The values of $n$ are almost constant (0.5) in all cases, regardless of the type of system under shear. However, the values of $k$ greatly depend on the system under consideration; the $k$ values decrease from high molecular weight polymer blends (PMMA/SAN) to simple liquid mixtures. This may be attributed to the fact that the effect of shear on the cloud points is much more sensitive in the high molecular weight polymer blends and that the sensitivity decreases in the simple liquid mixtures. From this result one can say that the sensitivity of the cloud points to the effect of applied shear rate in the different systems moves with the same order as the prefactor value in the different cases, with a greater value of the prefactor giving greater sensitivity of the cloud points to the application of shear rate. These reported results are in good agreement with a renormalization group theory of Onuki and Kawasaki (Onuki and Kawasaki 1979a, b; Onuki et al. 1981), who predicated the following equation for small molecular systems:

$$|\Delta T(\dot{\gamma})/T(0)| = p\dot{\gamma}^{1/3v} \tag{3}$$

where the prefactor $p$ is given by

$$p = 0.0832\varepsilon\tau_{\xi}{}^{1/3v} \tag{4}$$

and $\varepsilon = 4-d_s$ $1/3v = 0.5$ $v$ is a universal constant which depends on the spatial dimensionality $d_s$ $\tau_{\xi}$ is the characteristic relaxation time for the concentration fluctuations of the mixture. Equation 8.4 predicts that the larger the characteristic time ($\tau_{\xi}$) for the concentration fluctuations, the larger the change of the cloud point will be. This general principle can also be applied to a polymeric system, since the relaxation time decreases from the high molecular weight polymer mixtures to the simple liquid mixtures and becomes very small. Therefore, the large difference in the prefactor value, which reflects the sensitivity of the different systems to the shear rate, is not surprising at all.

According to this experimental fact, one can say that the phase behavior of the blend under shear flow can be changed due to the difference in the relaxation time, which reflects the different sensitivities of the cloud point to change under the shear flow.

### 8.3.4 PC/SAN Mixture (Immiscible System)

The blend of bisphenol-A polycarbonate (PC) and acrylonitrile-butadiene-styrene (ABS) resin is a useful industrial material. One reason is that the miscibility between PC and poly(styrene-*co*-acrylonitrile) (SAN), which is a matrix of ABS resin, is not too bad, though it is immiscible. In particular, a blend of PC and SAN-25 with 25 wt% AN is useful, because the miscibility is the best in PC/SAN systems and the blend shows the lowest value of $\chi$ in the system (Li et al. 1999). The blend has been used without any compatibilizers. It would be expected that the

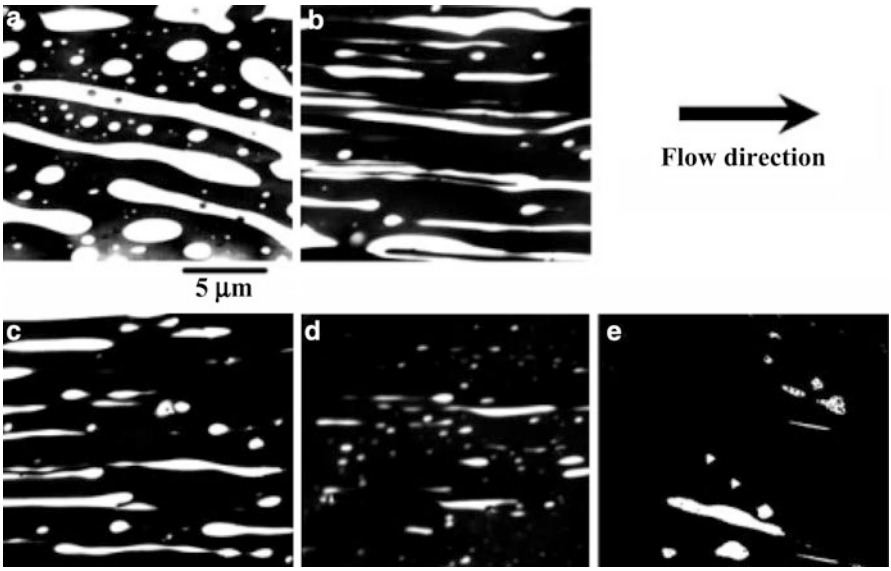


**Fig. 8.11** TEM pictures of PC/SAN-25 = 70/30 samples that were sheared at 240 °C by different shear rates for 5 min and then quenched in water bath. Five pieces were then taken from different radial positions and consequently different shear rates (**a**) $\dot{\gamma} \approx 0\ s^{-1}$; (**b**) 7.5 $s^{-1}$; (**c**) 15 $s^{-1}$; (**d**) 30 $s^{-1}$ and (**e**) 90 $s^{-1}$

miscibility of the blend might be more enhanced under the shear flow. The two-phase morphology under a controlled shear condition has attracted considerable attention in recent years. For this reason, the effect of simple shear flow on the morphology and miscibility of the PC/SAN-25 blend was investigated. A typical morphological observation of the blend samples (PC/SAN-25 = 70/30) under different values of the shear rate at 240 °C is shown in Fig. 8.11 (Hanafy et al. 2004). The bright dispersed phase and dark matrix correspond to the SAN-rich (not stained) and PC-rich (stained by $RuO_4$) regions, respectively. It is apparent that a well-defined phase separation of the blend at nearly zero shear rate can be obtained. For the samples under the shear flow, particles oriented to the flow direction were formed, and the size decreased with the shear rate. These results of TEM observation indicate that the size and amplitude of the concentration fluctuations between the domains and the surrounding matrix were strongly suppressed as a result of decreasing the contrast of the elongated domains. According to these results, one can say that the miscibility of the PC/SAN-25 mixture is enhanced to a great extent under the shear flow; i.e., the shear suppresses the concentration fluctuations and enhances the miscibility between different polymers. However, no shear-induced one-phase morphology was detected even under higher shear rate values. We must state here that the morphology under higher shear rate values (higher than 30 $s^{-1}$) does not change very much; see, for example, that at 90 $s^{-1}$ in Fig. 8.11e the morphology is almost similar to that at 30 $s^{-1}$ in Fig. 8.11d. This may be attributed to the fact that the sample under a higher shear rate seems to be

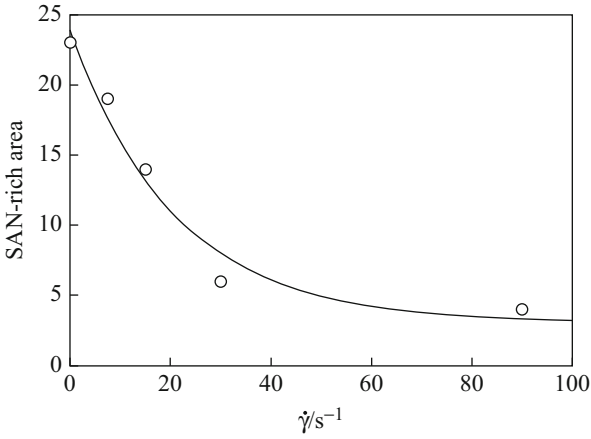


**Fig. 8.12** Shear rate dependence of the total area of SAN-rich phase

under a quasi-equilibrium condition. Based on this experimental fact, it is apparent that the morphology might be controlled by two competitive factors. One is trying to break up the domains into smaller ones, i.e., a shear-induced breakup of the dispersed domains. The other tends to increase the rate of domain growth, i.e., a shear-induced coalescence. The competition between the two factors is responsible for the obtained morphology. Therefore, the breakup is not a unique phenomenon involved during the shear flow, since coalescence of the dispersed particles also occurs, and the finally obtained morphology is the result of these two opposite effects.

Figure 8.12 shows the total area of the individual particles of the SAN-rich region as a function of the shear rate calculated from the image analysis of the previous TEM images (Fig. 8.11). Obviously, the area of the dispersed domains remarkably decreased with the shear rate and leveled off at high shear rates. As mentioned above, this is due to a competition of particle breakup and coalescence which may occur at high shear rate values.

Though the bisphenol-A PC is immiscible with SAN, as mentioned above, it was reported that a blend of a PC copolymer (cPC) and SAN-23 had a miscible region and showed an LCST-type phase diagram; see Fig. 8.13 (Okamoto et al. 1995). It was understood that the miscibility with SAN was enhanced by using random copolymer PC in comparison with the PC/SAN system. The LCST phase boundary shifts to higher temperatures by shearing, as shown in the figure, and the miscible region is enlarged, though the accurate amount is not clear quantitatively. The kinetic results provided a plausible scenario for the development of a co-continuous two-phase morphology in the melt-processed blend as follows. When the cold pellets of both polymers are heated to above the glass transition temperature (Tg) of the polymers in the extruder, the dissolution starts. Even after attaining the spinodal temperature of the quiescent state (Ts = 223 °C) the dissolution occurs continuously, since Ts can be elevated under the shear flow to above the barrel temperature (260 °C), shown as a dotted line in the figure. The homogeneous melt is extruded and quenched quickly in water. When the single-phase blend is heated under high shear in an injection machine (at 290 °C) and injected into a cold mold,

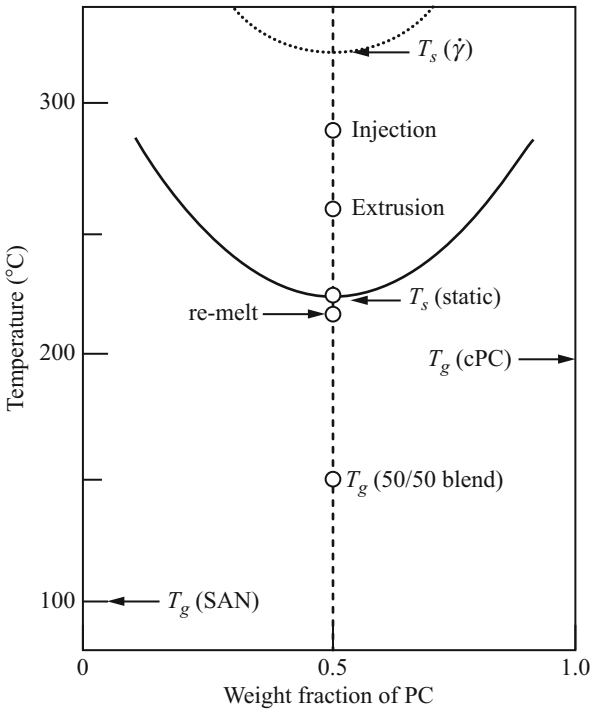


**Fig. 8.13** Phase diagram of cPC/SAN blend and processing conditions

the polymer blend is thrust into the two-phase region from the single-phase region, since the phase boundary returns to the lower temperature of the quiescent state without shearing. Then the spinodal decomposition proceeds until the melt is cooled to Tg. The dissolution below Ts is negligible, and so the co-continuous morphology attained via the spinodal decomposition is frozen in the molded blend by vitrification near Tg. Thus, one can obtain the co-continuous morphology in the polymer blends by controlling the shear field.

Figure 8.14 shows a TEM picture of an injection molding sample in the bisphenol-A PC/ABS blend (Inoue 1996). The black particles are rubber in the ABS-rich region. When one draws the boundary line between the rubber particle-rich region (ABS-rich) and the rubber particle-poor region (PC-rich), a co-continuous morphology appears. This may show that the morphology formation occurs via spinodal decomposition after single-phase formation by shearing in the PC/ABS blend. It might be the reason why the PC/ABS blend shows nice physical properties. This morphology control is extremely interesting.

### 8.3.5 PA4,6/PPS Mixture (Immiscible System)

Both nylon 4,6 (PA4,6) and poly(phenylene sulfide) (PPS) are useful industrial materials and have a high melting temperature of the crystals ($T_m$ = 295 °C and

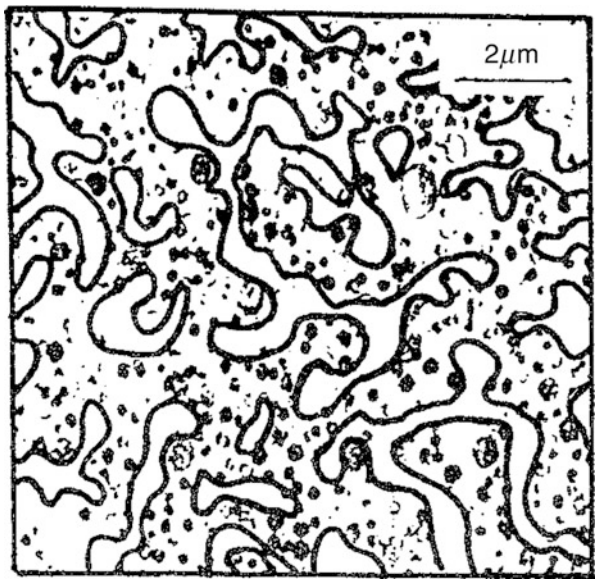


**Fig. 8.14** TEM picture of injection molding sample in PC/ABS (50/50). It is partitioned between overcrowdedness area (ABS-rich) of the rubber particle and white ground (PC-rich) by the line

280 °C, respectively). Therefore, we expect them to have the advantage that their polymer blend can maintain high temperature properties. The polymer blend of PA4,6/PPS has been used industrially without any compatibilizers; nevertheless, the blend is immiscible. Thus, it is considered that the shear flow during processing plays an important role for the formation of the phase-separated morphology related to the appearance of desirable properties.

The phase diagram at a quiescent state was confirmed in a liquid state from the melting temperature of the crystal to 400 °C by the cloud point measurement (An et al. 2002). The specimens were opaque and two-phase for every composition and measurable temperature. This means that the blend of PA4,6/PPS is immiscible in all processable regions. However, the specimen of PA4,6/PPS (80/20) in the higher shear rate region became transparent at 310 °C. The shear rate in the boundary of the opaque-transparent region was calculated ($\dot{\gamma} = 150\ s^{-1}$), and at higher shear rates than this value, the blend become miscible. This means that a shear-induced mixing took place in this blend. But a miscible region in other compositions could not be found. Figure 8.15 shows a phase diagram at $\dot{\gamma} = 150\ s^{-1}$ and $\dot{\gamma} = 189\ s^{-1}$. A miscibility region (window) can open by the shear flow, though it is very narrow.

Figure 8.16a shows an optical micrograph of a PA4,6/PPS(80/20) specimen annealed at 310 °C for 10 min after the cessation of the shear flow, which was one phase under shear flow ($\dot{\gamma} > 150\ s^{-1}$) at the same temperature. A regularly and co-continuously phase-separated structure appears. Figure 8.16b shows a light scattering profile exhibiting a peak due to the regular morphology. It seems that phase separation took place via spinodal decomposition from one phase state after the cessation of shear flow. Such a fine morphology in polymer blends often causes good physical properties.

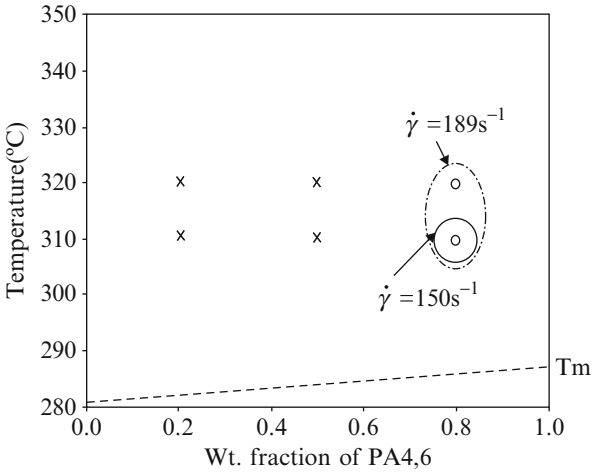


**Fig. 8.15** Phase diagram of PA4,6/PPS blend under simple shear flow. The lines of phase boundary at $\dot{\gamma} = 150\ s^{-1}$ and $\dot{\gamma} = 189\ s^{-1}$ are drawn arbitrarily because the shape of phase diagram is not clear at present

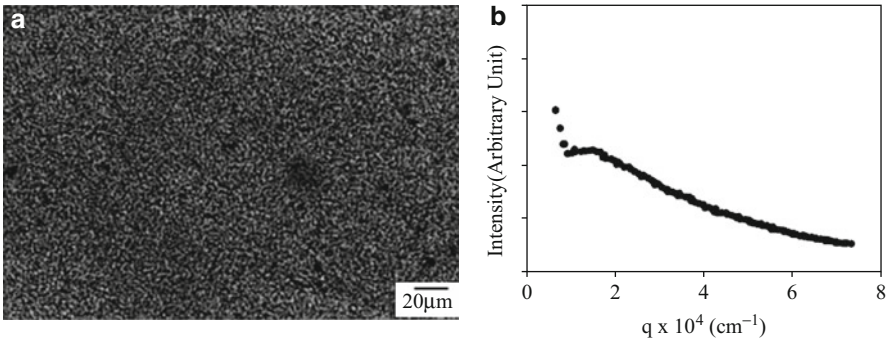


**Fig. 8.16** (**a**) Optical micrograph of PA4,6/PPS (=80/20) blend annealed in hot chamber for 10 min at 310 °C after shear cessation. Co-continuous morphology appeared. (**b**) Light scattering profile of this sample

To conclude, the miscibility of the PA4,6/PPS blend changed with the shear flow, and a miscible region appeared. By using this phenomenon, a specimen with a fine morphology and good physical properties could be obtained.

## 8.4 Reaction-Induced Phase Separation

There are several methods used to mix polymers. Reaction-induced phase separation (RIPS) is one way to make useful polymer blends, and much research has been previously done on this topic (Visconti and Marchessault 1974; Manzione et al. 1981; Yamanaka and Inoue 1989, 1990; Yamanaka et al. 1989; Chen et al. 1994; Okada et al. 1995; Kojima et al. 1995; Inoue 1995). As explained before, many polymer blends are immiscible, and it is difficult to make them form a desirable

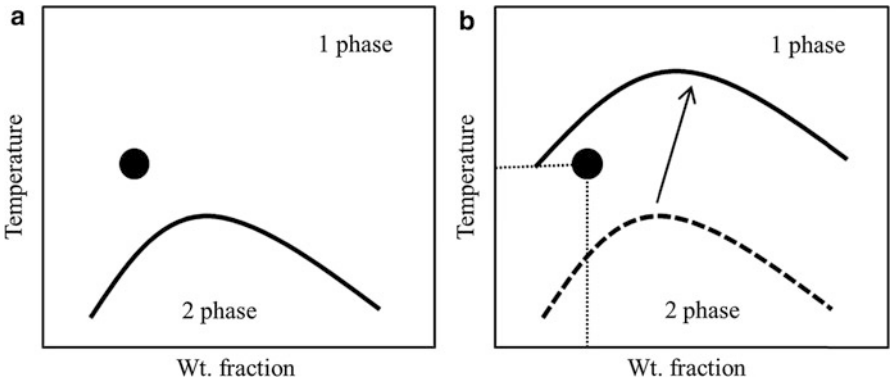


**Fig. 8.17** Schematic representation of phase diagram in polymer blend with polymerization; (**a**) monomer/polymer blend before polymerization, (**b**) polymer/polymer blend after polymerization. *Solid circle* (●) represents polymerization condition

phase-separated morphology. RIPS occurs as a result of a curing reaction (c-RIPS) and polymerization of a monomer (p-RIPS) after one polymer is dissolved in another monomer forming a homogeneous solution initially. The phase separation is induced in the process of curing or polymerization of the monomer. Because the phase separation occurs from one phase state, it often occurs by the spinodal decomposition (SD) mechanism, and a regular phase-separated morphology is formed in the initial stage of the phase separation. Therefore, it is easy to obtain a material with a better performance. However, in RIPS, the obtained final morphology is remarkably different from that obtained by the usual phase separation of the binary polymer-polymer blends. Interest in the morphology of the blends obtained by RIPS has led to many research studies in this area.

Here the phase separation phenomenon by p-RIPS is explained by using the Flory-Huggins equation expressed by Eq. 8.1. Generally, if the interaction parameter $\chi_{12}$ is independent of the number of segments per chain, the miscibility during the polymerization is dominated by the number of segments in the combinatorial entropy terms on the right side of Eq. 8.1. That is, the larger the degree of polymerization, the narrower the miscible region becomes. Figure 8.17 shows the schematic representation of a UCST-type phase diagram in a blend: (a) the monomer/polymer blend before polymerization and (b) the polymer/polymer blend after polymerization. The solid circle in the phase diagram represents the position of the polymerization condition. When the degree of polymerization in a polymerized component is small, the system locates at the miscible state before the polymerization (Fig. 8.17a). The degree of polymerization becomes large as the polymerization proceeds, and the combinatorial entropy terms become negligible. Because the free energy of mixing becomes larger, the phase boundary shifts to the higher temperature with polymerization, as shown in Fig. 8.17b. Consequently, the system is thrust into a two-phase region from a one-phase region. Then, the phase separation occurs.

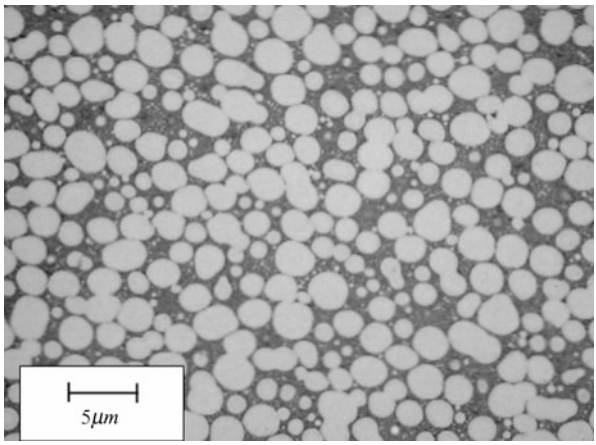


**Fig. 8.18** TEM micrograph of PMMA/EVAc(80/20) blend polymerized at 60 °C

It has been reported that this phenomenon has been observed in the radical polymerization of methyl methacrylate (MMA) in the presence of poly(ethylene-*co*-vinyl acetate) (EVAc) (Chen et al. 1994). The MMA/EVAc blend shows a UCST phase diagram, and the shift of the phase diagram with polymerization of MMA is the same as that in Fig. 8.17. Figure 8.18 shows a TEM micrograph of the PMMA/EVAc (80/20) blend prepared by p-RIPS. The bright region is assigned to the polymerized PMMA region. The phase-separated structure shows a unique morphology in which the particles of the major component (PMMA) were dispersed in a matrix of the minor component (EVAc). Also, this blend prepared by polymerization shows a high impact strength. Figure 8.19 shows the notched Izod impact strength of PMMA/EVAc blends obtained by p-RIPS and melt-blending (Kojima et al. 1995). The blends obtained by polymerization show much higher impact strength than those by melt-blending. This result may be caused by the phase separation morphology in which the EVAc region with a rubbery property forms a matrix regardless of the minor component. This PMMA/EVAc blend obtained by polymerization is put to practical use because of its good physical properties.

As an example of c-RIPS, an epoxy/poly(ether sulfone) (PES) system with a phase diagram exhibiting an LCST behavior was demonstrated in Fig. 8.20 (Yamanaka and Inoue 1989). The binary mixture was first homogeneous at the curing temperature (below LCST). During the curing process, the system was thrust into a two-phase region by the LCST depression caused by increase of the molecular weight or the conversion, and the phase separation was expected to take place via SD. In this particular system, the progress of decomposition will eventually be suppressed by the vitrification, as shown by the approaching $T_g$ line and by gelation in the epoxy-rich region. The morphology of the phase-separated structure in c-RIPS yields a variety of two-phase structures – interconnected globule structure, droplet structure with uniform domain size, and bimodal domain structure, depending on the relative rates of the chemical reaction and the phase separation (Yamanaka and Inoue 1989). Figure 8.21a shows a scanning electron

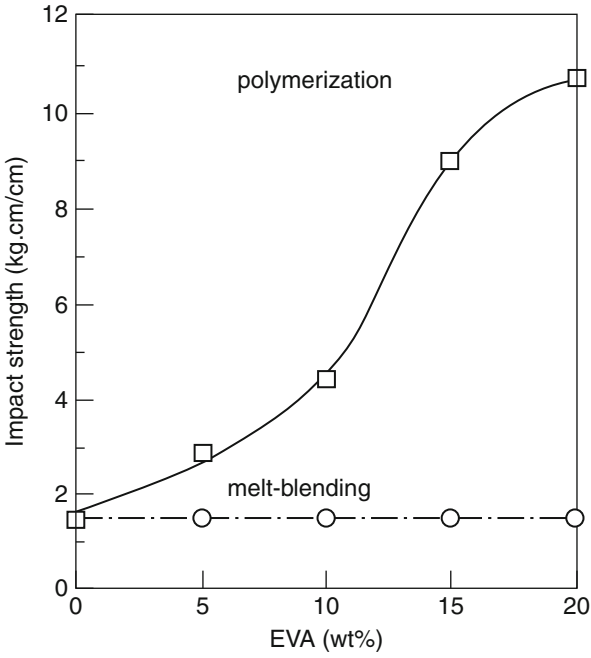


**Fig. 8.19** Notched Izod impact strength of PMMA/EVA blend prepared by p-RIPS and melt blending

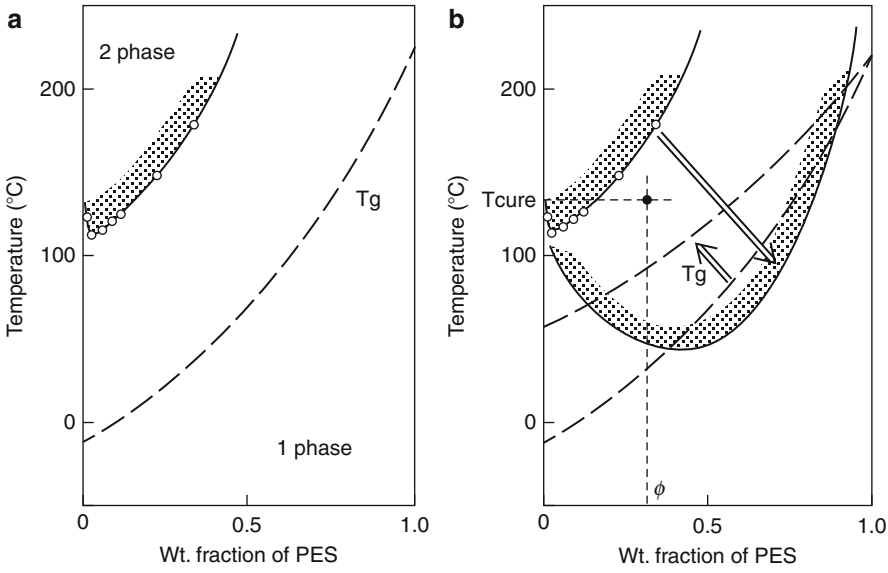


**Fig. 8.20** (**a**) Phase diagram of epoxy oligomer/PES system. (**b**) Schematic representation of the variation of the phase diagram and Tg with curing. *Solid circle* (●) represents curing condition

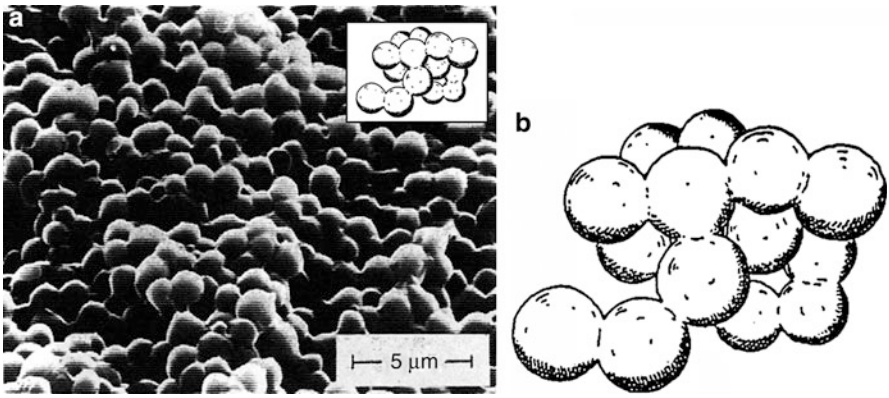


**Fig. 8.21** SEM micrograph of cured resin epoxy/PES; PES 50 phr, 170 °C, 3 h

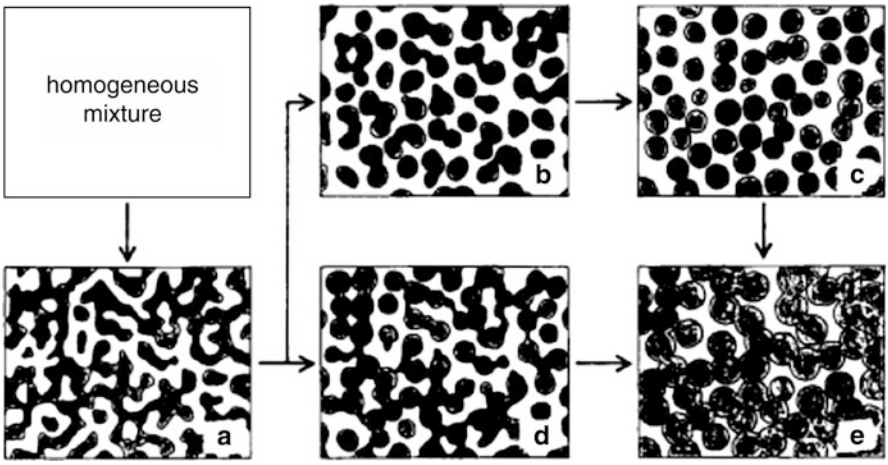


**Fig. 8.22** Schematic representation of phase separation process resulting in connected-globule structure

microscope (SEM) micrograph for the cured resin in the epoxy/PES (100/50) system. Fine globules which are fairly uniform in size (a few micrometers) are seen. Furthermore, the particles seem to be connected to each other (Fig. 8.21b). This connected-globule structure implies a two-phase morphology of the interconnected spherical domains of the epoxy-rich phase of a major component dispersed regularly in a matrix of PES. This kind of morphology can never be obtained by mixing two polymers with an asymmetrical blend composition. The schematic representation of the changes in the phase separation structure is shown in Fig. 8.22 (Yamanaka and Inoue 1989). The dark region is assigned to the epoxy-rich region. During this curing reaction the homogeneous blend starts to phase-separate by SD (Fig. 8.22a). When the phase separation proceeds, the dispersed droplet-type

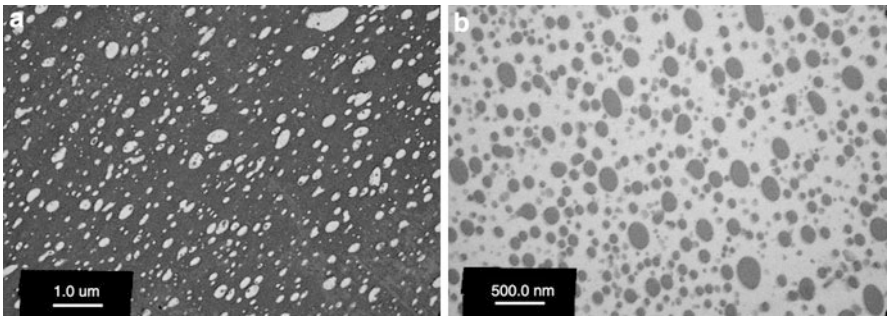


**Fig. 8.23** TEM micrographs of the blends mixed by the mechanical blending at 200 °C for 5 min (**a**) PS/PMMA(80/20), (**b**) PMMA/PS(80/20)

morphology (Fig. 8.22b, c) or network morphology which is established with droplets (Fig. 8.22d) appears. The coarsening of domains then proceeds, eventually resulting in the connected-globule structure (Fig. 8.22e). The epoxy-rich region and PES-rich region form the domain and matrix, respectively. In polymer/polymer blend systems, generally the major component becomes the matrix while the minor component becomes the domain. However, in c-RIPS, the domain phase is formed by the cured component even if the cured component is major. This epoxy/PES system has good adhesive properties such as high peel strength because of this morphology.

Thus, the scenarios are plausible in the explanation of c-RIPS with the curing process. However, there was no explanation why the major component could form the domain in both of p-RIPS and c-RIPS. Also, so far the formation mechanism of the phase-separated morphology has apparently not been elucidated. Therefore, the following model experiments were carried out.

### 8.4.1 p-RIPS in PS/PMMA Systems

As a model blend of p-RIPS, the PS/PMMA systems were investigated. Both polymers are easily synthesized by radical polymerization from the monomer (Ono et al. 2008). This polymer blend is immiscible, but shows a small value of the positive interaction parameter, $\chi$. The morphologies of the polymer blends mixed mechanically at 200 °C for 5 min are shown in Fig. 8.23a and b. The TEM micrographs are of PS/PMMA (80/20) and PMMA/PS (80/20), respectively. The darker regions correspond to the PS-rich phase and the brighter regions are associated with the PMMA-rich phase, because the phenyl group of PS is more stained by $RuO_4$. As shown in the figures, the minor component forms the domain in the major component matrix. In fact, in the case of PS/PMMA (80/20), PMMA, the minor component, was dispersed in the PS matrix as small domains after the mechanical melt blending. Phase inversion occurred in PMMA/PS (80/20) as a matter of course. The minor component of PS then formed many small domains. This phenomenon occurred predictably as is known in the field of polymer blends.

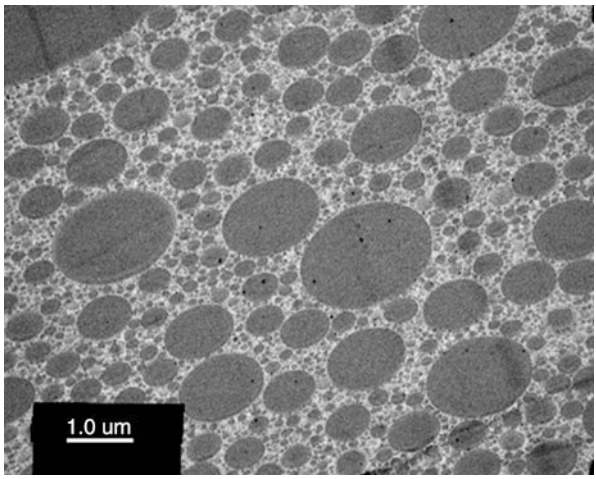


**Fig. 8.24** TEM micrographs of the phase-separated structure of styrene/PMMA/AIBN(80/20/0.2) blend after polymerization at 80 °C in polymerization-induced phase separation

The final morphology of the binary blend prepared via p-RIPS is greatly different from that prepared via mechanical melt blending with the polymers, as stated above. The polymerized component tends to form the domains regardless of the varieties of monomer and reaction.

Here, not only styrene/PMMA (80/20) but also MMA/PS (80/20) could be prepared to observe the morphology obtained by p-RIPS. The process of the phase separation was observed by optical microscopy (OM) and light scattering (LS) measurements during the polymerization. The final morphology was observed by TEM, and image processing was carried out for the micrographs obtained by OM and TEM.

#### 8.4.1.1 Styrene/PMMA Mixture

PMMA was dissolved in the styrene monomer with a radical initiator, α,α′-azobis (isobutyronitrile) (AIBN). Figure 8.24 shows the TEM micrograph for PS/PMMA/AIBN (80/20/0.2) after a polymerization of styrene completely finished at 80 °C. The brighter regions are associated with the PMMA-rich phase and the darker regions correspond to the PS-rich phase. According to this micrograph, the PS-rich phase formed the domains, although PS is the major component in this blend system, and the PMMA-rich phase formed the continuous phase in spite of being 20 wt% in content. This unique morphology can never be obtained by mechanical melt blending in binary polymers. As mentioned above, the minor component will form domains in mechanical melt blending. To confirm the particularity, the polymerized specimen was blended again by melt mixing. Of course, it was observed that the PMMA-rich phase of the minor component formed small domains in the PS-rich phase matrix of the major component, quite the same as in Fig. 8.23a. Furthermore, referring in detail to Fig. 8.24, there are several types of domains with different sizes, of which the larger domain is 10 μm and the smaller domain is 10 nm in diameter.

To investigate the formation process of the phase-separated morphology, the LS measurement and the observation by OM were carried out during the polymerization

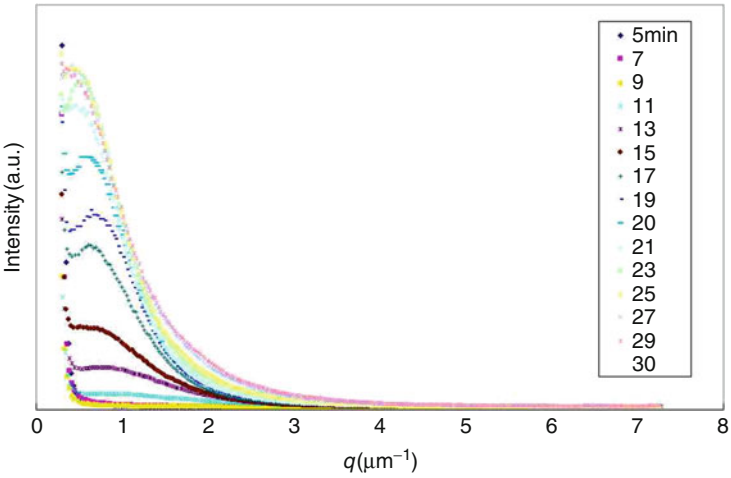


**Fig. 8.25** Change of light scattering profiles in the process of the polymerization of sty/PMMA/AIBN (80/20/0.2) mixture at 80 °C

at 80 °C for a styrene/PMMA/AIBN (80/20/0.2) mixture. This mixture was homogeneous in solution between room temperature and the polymerization temperature (80 °C).

Figure 8.25 shows the time-resolved LS profiles during the process of the polymerization of the styrene/PMMA/AIBN (80/20/0.2) mixture at 80 °C. The scattering vector is defined by

$$q = \frac{4\pi}{\lambda} \sin \frac{\theta}{2} \tag{5}$$

where $\lambda$ and $\theta$ are the wavelength of light in the medium and the scattering angle, respectively. The light scattering occurred slightly after a certain time lag of ~9 min, then one peak started to appear at $q = 0.7\ \mu m^{-1}$ after 11 min. The peak implied the development of a regularly phase-separated morphology. From these profiles, one can estimate the periodic distance, $\Lambda_m$, in the phase-separated morphology using a Bragg equation and the scattering vector:

$$\Lambda_m = \frac{2\pi}{q} \tag{6}$$

The periodic distance was estimated to be 9 μm when the peak appeared first. However, this distance is too large for that in the initial stage of spinodal decomposition (SD) because the periodic distance in a typical SD is usually of submicron order in the case of polymer-solvent and polymer-polymer systems. This implies that this phase separation may not be occurring via SD. Therefore, an observation by OM was carried out to investigate the morphology at the early stage of the phase separation.

Figure 8.26 shows the optical micrographs observed at the various stages of polymerization at 80 °C. After about 8 min from the starting of polymerization of styrene monomer, the phase separation started to occur but with low contrast. A domain having a uniform particle size was generated at irregular positions like a morphology formed by the nucleation and growth (NG) mechanism. A co-continuous morphology was not observed in this blend system. Coarsening of the domains took place with time up to 15 min. In addition, the second phase separation was observed to occur in the matrix phase at 15 min. After that, collision and coalescence between the domains took place, and the two types of domains simultaneously coarsened with time. These optical micrographs indicated that the several phase separations took place in many stages in this blend system. Furthermore, it was confirmed that these step-by-step phase separations do not occur via SD-type but rather by NG-type processes.

The size distribution of domains in the phase-separated morphology in the picture of OM or TEM was estimated after threshold by image processing with the software Image J in order to investigate the change of the volume fraction and particle size with time. From this image analysis, the small domains generated at the initial stage (8 min) coarsened gradually, and then another phase separation was observed at 15 min with the advent of the bimodal distribution. Therefore, this indicates that the two phase separations occurred in steps in this system. Figure 8.27 shows the time dependence of particle diameter in a two-step phase separation. The smaller particle size generated in the second phase separation agreed with that of the domains generated in the first phase separation. Figure 8.28 shows the time dependence of the volume fraction of the polymerized major component, the PS-rich phase, by adding the values of each phase separation step. Because the area of the PS-rich region is almost 73 % of the TEM image of Fig. 8.24, which is a final morphology, it is considered that at least three steps of the phase separation occur.

It is possible to think about the phase separation in this system from the above discussion by looking at Fig. 8.29, which is the schematic diagram showing the triangle phase diagram of the styrene/PMMA/PS system at 80 °C. Since the PMMA content was fixed at 20 wt%, the initial binary solution of styrene/PMMA is indicated by the black filled circle. The polymerization process can be described by the arrow. Polymerization of styrene causes the solution to enter the two-phase region in which it separates into two phases, one rich in polymer PMMA and the other rich in generated polymer PS. The phase separation in the metastable region should proceed by the NG mechanism. Furthermore, the second phase separation took place in the PMMA-rich phase via NG. In this way, the several processes in the step-by-step phase separation are assumed to induce the unique phase-separated morphology. From this phase diagram, in the first phase separation, the PS-rich phase is minor and the PMMA-rich phase is major by the principle of leverage. The second phase separation occurs in the PMMA-rich phase, which is major, and it is repeated. Therefore, it is difficult for the domains to collide and coalesce with each other, and the coarsening of domains might be suppressed. As a result, the many PS-rich domains disperse in the matrix regardless of the major component until the polymerization finishes completely. Perhaps this is a reason why the PS which is a major component forms a domain.

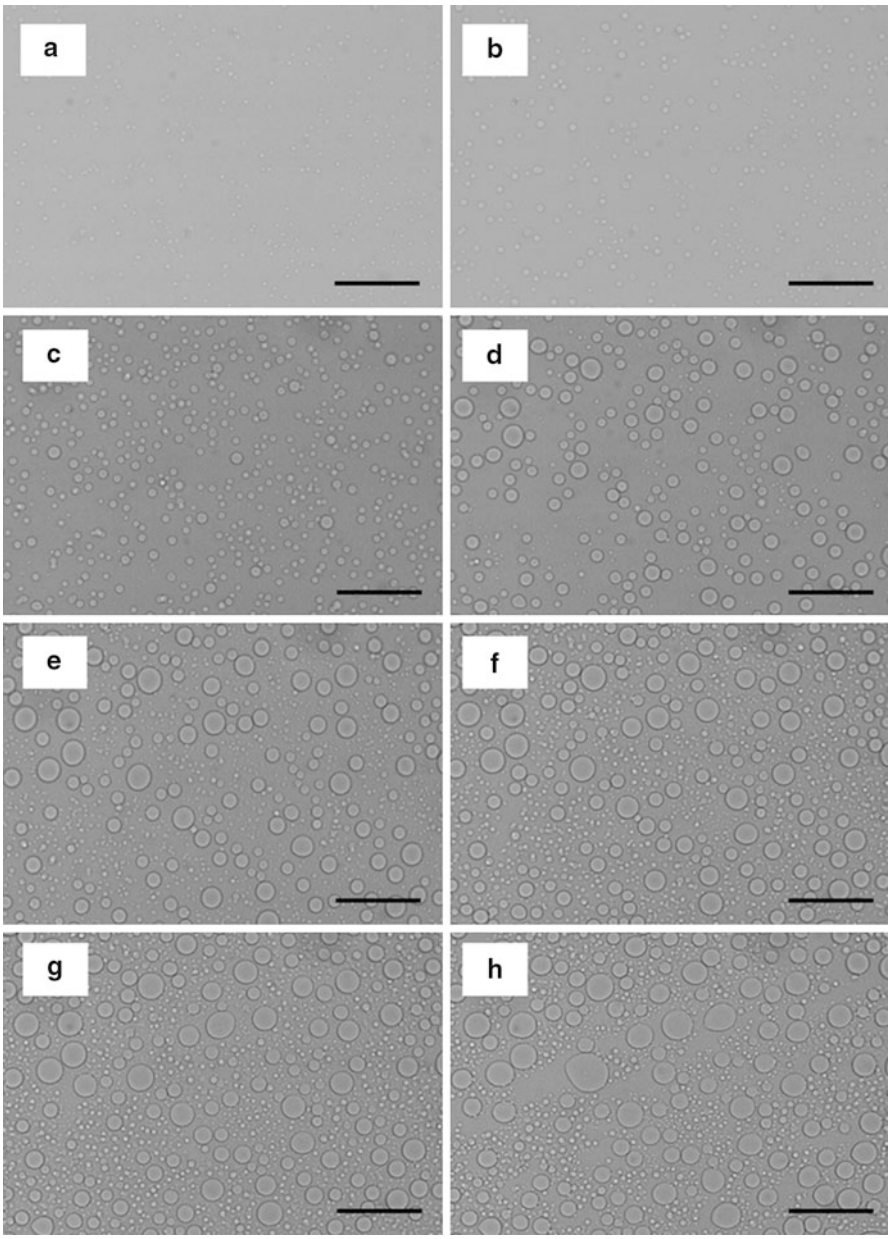


**Fig. 8.26** Optical micrographs at various stages of polymerization of sty/PMMA/AIBN(80/20/0.2) at 80 °C. Scale bar: 50 μm (**a**) 8 min (**b**) 10 min (**c**) 13 min (**d**) 15 min (**e**) 20 min (**f**) 25 min (**g**) 30 min (**h**) 35 min

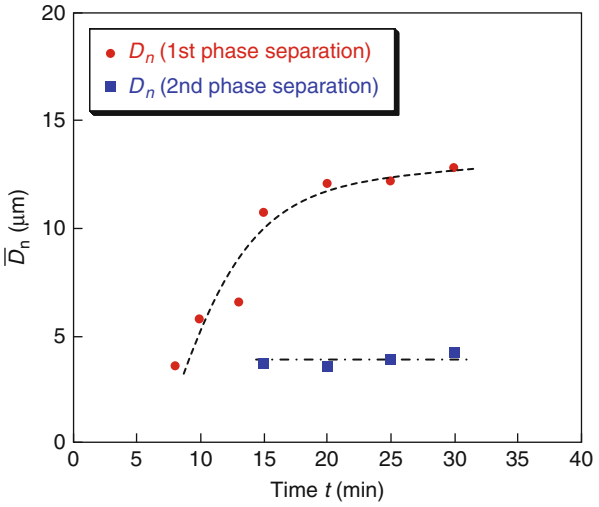


**Fig. 8.27** Number-average particle diameter $D_n$ vs time in sty/PMMA/AIBN(80/20/0.2) blend during polymerization at 80 °C. (●) Number-average particle diameter of PS-rich domains at 1st phase separation (■) at 2nd phase separation

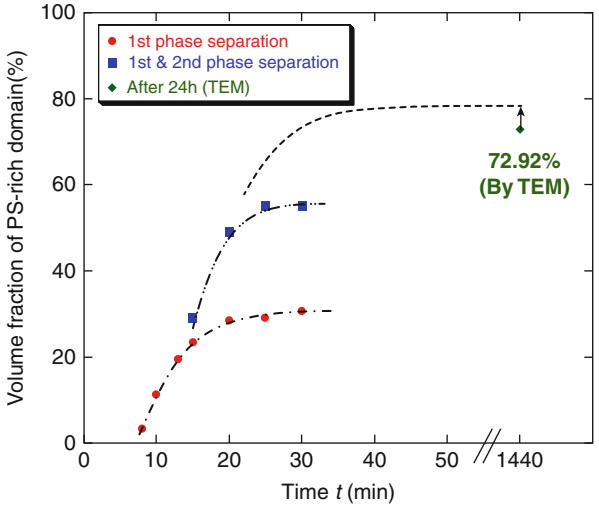


**Fig. 8.28** Change of volume fraction of PS-rich domain in sty/PMMA/AIBN(80/20/0.2) blend during polymerization at 80 °C. (●) Volume fraction of PS-rich domains at 1st phase separation, (■) 1st & 2nd phase separation

### 8.4.1.2 MMA/PS Mixture

Figure 8.30 shows a TEM micrograph for MMA/PS/AIBN (80/20/0.2) after polymerization of MMA completely finished at 80 °C. The brighter regions are associated with the PMMA-rich phase and the darker regions correspond to the PS-rich phase. According to this micrograph, the PMMA-rich phase formed the domains, although PMMA was a major component in this blend system, and the PS-rich phase formed the continuous matrix phase in spite of being 20 wt% content. This morphology is opposite to the morphology seen in the styrene/PMMA/AIBN (80/20/0.2) system as shown in Fig. 8.24.

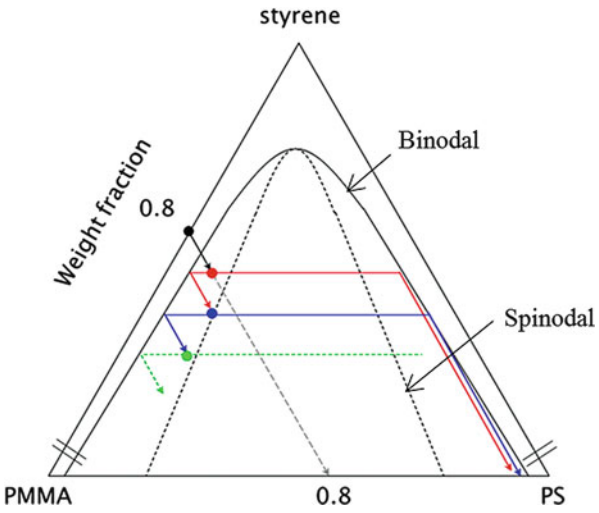


**Fig. 8.29** Triangle phase diagram of styrene/PMMA/PS system at 80 °C. Spinodal and binodal curves are by *broken* and *solid lines*, respectively. *Arrow* indicates the polymerization process

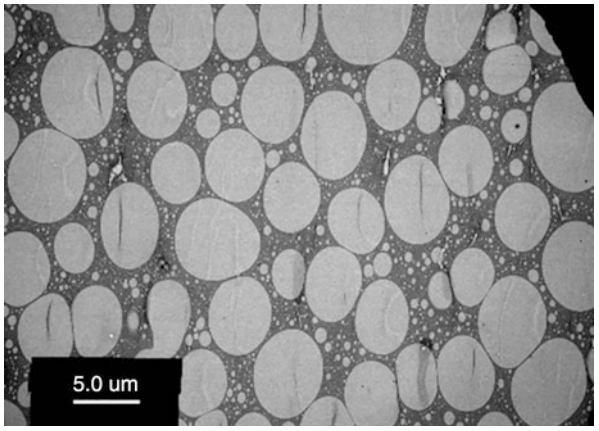


**Fig. 8.30** TEM micrograph of the phase-separated structure of MMA/PS/AIBN (80/20/0.2) blend after polymerization at 80 °C in p-RIPS

To investigate the formation process of the phase-separated morphology, the measurement of LS and the observation by OM were carried out. Figure 8.31 shows the time-resolved LS profiles during the process of the polymerization. The periodic distance $\Lambda_m$ was estimated to be about 2.1 μm. The position of the peak started to shift toward a smaller angle as the polymerization progressed. The phenomenon revealed the occurrence of coarsening of the periodic structure at the late stage of the SD mechanism.

The change of the volume fraction of the PMMA-rich phase and the periodic distance $\Lambda_m$ of the co-continuous morphology versus time can be estimated from the optical and TEM micrographs after threshold by the image processing with the software Image J (see Fig. 8.32). The black region is associated with the PMMA-rich phase. The pictures after the image processing clearly represent

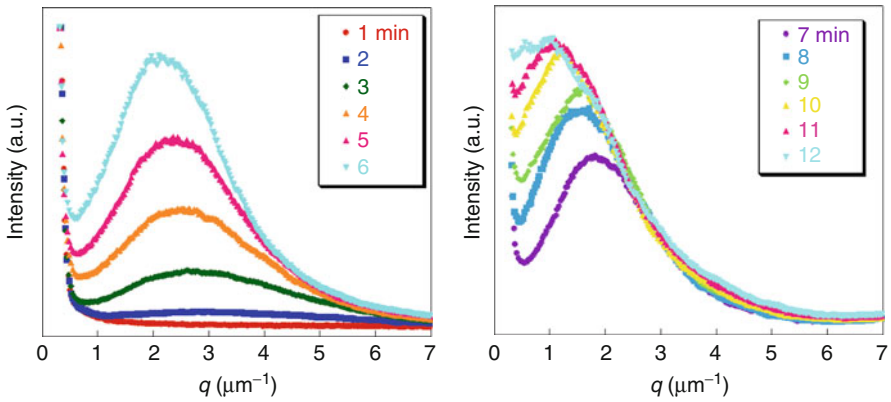


**Fig. 8.31** Changes of light scattering profiles in the process of the polymerization of MMA/PS/AIBN (80/20/0.2) mixture at 80 °C

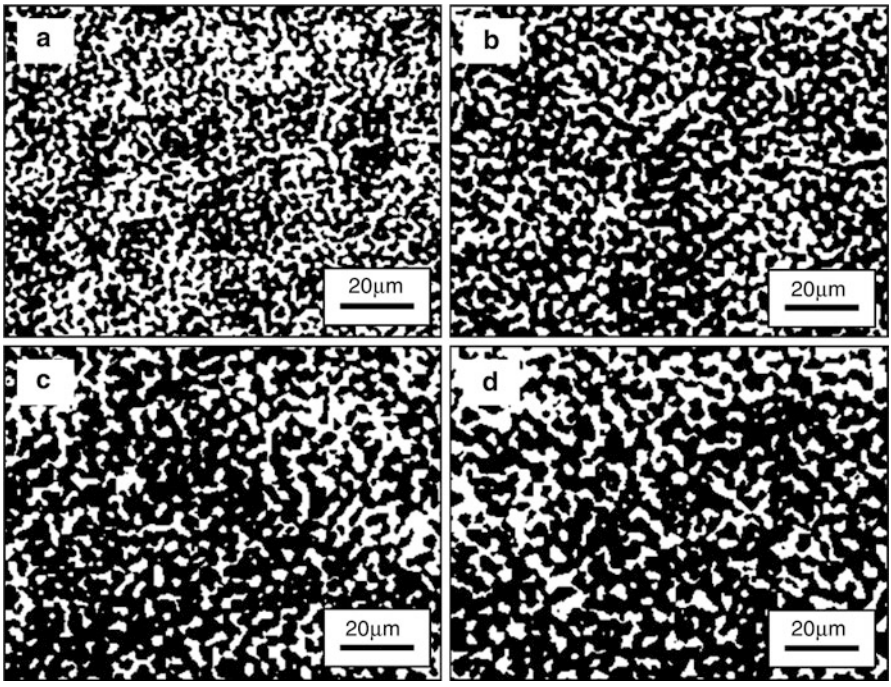


**Fig. 8.32** Optical micrographs after image processing at various stages of polymerization of MMA/PS/AIBN(80/20/0.2) at 80 °C. (**a**) 10 min (**b**) 15 min (**c**) 20 min (**d**) 25 min

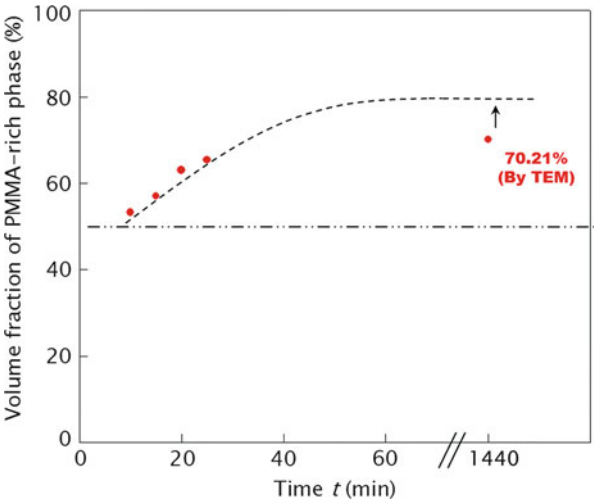


**Fig. 8.33** Time dependence of volume fraction of PMMA-rich phase in MMA/PS/AIBN (80/20/0.2) blend during polymerization at 80 °C

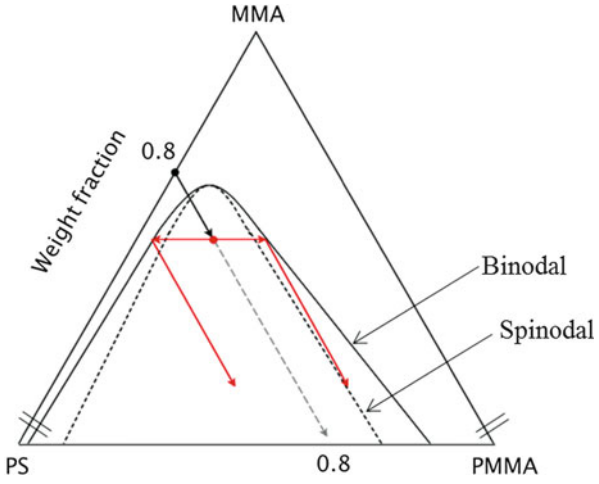


**Fig. 8.34** Triangle phase diagram of MMA/PS/PMMA system at 80 °C. Spinodal and binodal curves are by *broken* and *solid lines*, respectively. *Arrow* indicates the polymerization process

the co-continuous structure via the SD. Furthermore, the coarsening behavior of the periodic morphology was observed. This indicates that the volume fraction of the PMMA-rich phase increased gradually with time (Fig. 8.33). The volume fraction should approach 80 % of the mixing composition if the phase separates to pure PS and pure PMMA completely. However, it does not completely correspond because there are many small particles which were not recognized by the image processing, or perhaps the phases do not separate pure components.

It is possible to think about the phase separation in this system from the above discussion by looking at Fig. 8.34, which is the schematic diagram showing a triangle phase diagram of the MMA/PMMA/PS system at 80 °C. Since the PS weight fraction was fixed at 20 wt%, the initial binary solution of MMA/PS is

indicated by a black filled circle. The polymerization process can be described by the arrow. The binodal and spinodal lines shift to the PS-rich side in some measure, as shown in Fig. 8.34, because the MMA/PS/AIBN (90/10/0.225) system did not show phase separation after polymerization of MMA at 80 °C. However, we suppose that the blend system did not cause the phase separation and was frozen at the miscible state because the sample entered the two-phase region late during the process of polymerization which is a low mobility stage. From the above results, this phase separation took place in the spinodal region in the triangle phase diagram. Therefore, the volume fraction of the formed domain is supposed to be almost 50 % derived from the concentration fluctuation in the co-continuous morphology at the initial stage of SD. After that, the volume fraction of the PMMA-rich phase increases up to near 80 % that is the mixing composition. However, the PMMA-rich phase, which is the major component, forms domains in the late stage of the phase separation. Because the volume fraction of each phase in the initial stage of the phase separation should be almost even, one cannot explain this result as explained in the NG mechanism for styrene/PMMA/AIBN (80/20/0.2). Therefore, it is considered that the polymerization process induced the change of the coarsening mechanism and the formation of a unique morphology in p-RIPS.

Which phase wants to form domains after the co-continuity is lost? Considering that this unique morphology is never formed by conventional thermal-induced phase separation, it is thought that changes of some kind of physical properties induced by the polymerization cause it. There are changes in physical properties, such as viscoelasticity and volume shrinkage. The answer is not clear at present.

## 8.5 Reactive Blending

The reactive blending of immiscible polymers yields a block or graft copolymer at the interface. By an emulsifying effect of the in situ-formed copolymer, the dispersed particles can be reduced down to submicrometer size, and the interfacial adhesion can be improved. Then, the material properties are improved. It may be a commonly accepted story for compatibilization (Baker et al. 2001). In addition to the emulsifying effect, new interfacial behaviors of the in situ-formed copolymers have been found recently; such as pull-out and pull-in of copolymers by the external shear forces. These render a series of high-performance materials with new morphologies. Further, a new approach has been explored by combining many reactions, e.g., coupling and exchange reactions.

### 8.5.1 Coupling Reaction at Polymer-Polymer Interface

The first example of reactive blending is a system containing polyamide (PA-6) and polypropylene (PP) with a small amount of maleic anhydride (MAH) (Ide and Hasegawa 1974). A coupling reaction between the amino chain end of PA with MAH leads to the in situ formation of a PA-PP graft copolymer at the interface (see Fig. 8.35).

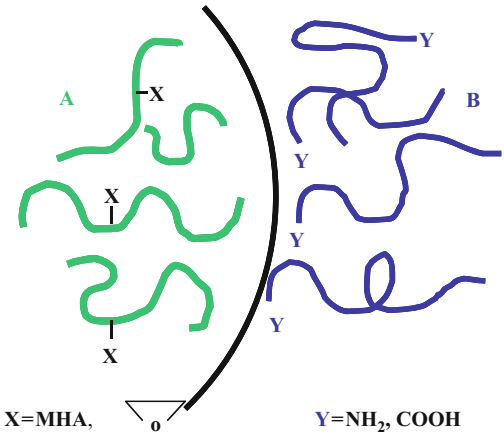


**Fig. 8.35** Polymer-polymer interface as the reaction site

The coupling reaction proceeds very quickly, caused by concentrating the reactive moieties (MAH, epoxide, $NH_2$, COOH, etc.) at the interface. The polymer chain end generally prefers to locate at the interface, because such a chain conformation is more probable, compared with the case where a mid-segment locates near the interface. Then, the amino chain ends of PA may be concentrated at the interface. The MAH unit is highly polar and is unstable in the non-polar PP-MAH phase, and it tends to segregate at the interface to contact with the polar chain of PA. Thus, both reactive sites may be concentrated near the interface to provide a favorable situation for the coupling reaction.

This type of blending has been used to produce the "super-tough nylon" PA/poly (phenylene ether) (PPE) alloy (Baker et al. 2001). Similar reactive blending of PPE with poly(ethylene-*co*-glycidyl methacrylate) (EGMA) yields a high-temperature engineering plastic with low dielectric loss and nice melt-processability (Furuta et al. 2007). It can be classified as a super-engineering plastic, like poly(ether sulfone) and poly(ether imide). A super-ductile alloy with excellent high-temperature resistance was also developed by reactive blending of poly(butylene terephthalate) (PBT) with EGMA (Hashima et al. 2008).

### 8.5.2 In situ-formed Copolymer as an Emulsifier

The in situ-formed copolymers locate at the interface to prevent coalescence of the dispersed particles. The brush chains (the B chains of the in situ-formed A-B copolymer; see Fig. 8.35) on the dispersed particles overlap when neighboring particles approach each other. By the chain overlap, the conformational entropy decreases to generate a repulsive interaction between the particles, which is different from the electrostatic repulsion in low molecular weight systems (oil/water/soap).

The emulsifying effect of the in situ-formed copolymers allows a fine dispersion to be achieved by reactive blending. The particle size during reactive blending of

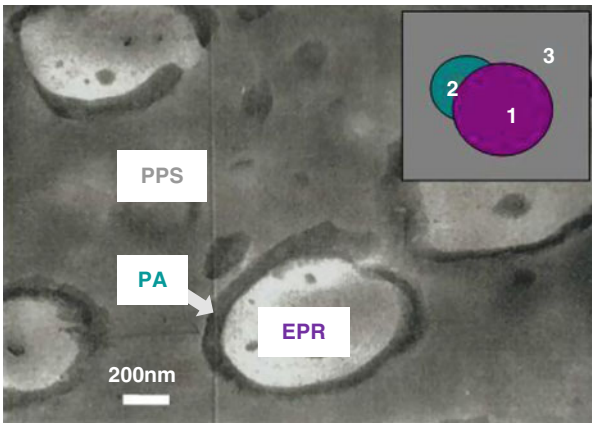


**Fig. 8.36** TEM of PPS alloy toughened by the encapsulation of EPR particles by PA

PA-6 and MAH-functionalized polystyrene (PS) decreased by two orders of magnitude, in comparison to the nonreactive PA-6/PS = 80/20 (Park et al. 1992). The change in the morphological parameters, such as the mean radius of dispersed particles and the specific interfacial area, with mixing time was quantitatively shown as a function of reaction time via light scattering analysis (Okamoto and Inoue 1993).

The in situ-formed copolymer reduces the interfacial tension. In ternary systems of a major component (3) and two minor components (1 and 2), as schematically shown in Fig. 8.36, component 2 spreads over the component 1 particles when the spreading coefficient $S$, determined by a balance between the interfacial tensions $\Gamma_{i/j}$, is positive. The $S$ in a ternary system of EPR (ethylene-propylene rubber) (1)/PA(2)/PPS (poly(phenylene sulfide)) (3) defined by

$$S = \Gamma_{\mathrm{PPS/EPR}} - \Gamma_{\mathrm{PA/EPR}} - \Gamma_{\mathrm{PPS/PA}}$$

can be positive when the value of $\Gamma_{\mathrm{PPS/PA}}$ is reduced by the formation of an in situ-formed copolymer of PPS and PA. Then, PA shell-EPR core particles are dispersed in a PPS matrix, as shown in Fig. 8.36. The formation of the core-shell particles gives the ternary alloy high toughness, even when the surface-to-surface interparticle distance $\tau$ is fairly large ($\tau$ = 500 nm) (An et al. 2001).

### 8.5.3 Pull-out of in situ-formed Copolymer

During reactive blending, the in situ-formed copolymers are sometimes pulled out from the interface and dispersed as micelles (domains) in the matrix, as shown in Fig. 8.37. The micelles are typically 20 nm in diameter (Ibuki et al. 1999). The pull-out does not occur at the static state; i.e., it is not caused by the interfacial instability of the highly crowded copolymers themselves. The pull-out takes place mechanically under the shear fields (Charoensirisomboon et al. 1999).

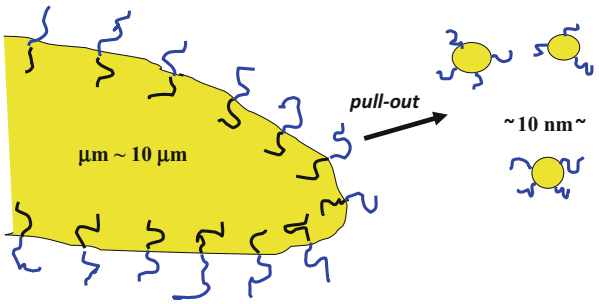


**Fig. 8.37** Pull-out of in situ-formed block copolymer

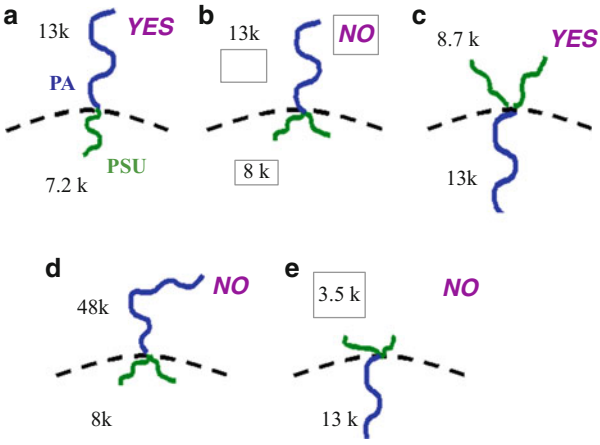


**Fig. 8.38** In situ-formed copolymers are pulled out (YES) or not pulled out but stay at interface (NO), depending on the molecular architecture. Figures are number average molecular weight of component polymers

Whether pull-out occurs or not highly depends on the molecular architecture, as shown in Fig. 8.38 (Charoensirisomboon et al. 2000). A block copolymer with a linear structure is easily pulled out (YES, Fig. 8.38a). An in situ-formed graft copolymer with a trunk chain located in the dispersed particle (inverse-Y shape) is hardly pulled out and plays the role of emulsifier (NO, Fig. 8.38b). By contrast, a graft copolymer with a trunk chain in the matrix (Y shape) can be pulled out easily (Fig. 8.38c). An inverse-Y shaped graft copolymer is hardly pulled out, even in the case of a short trunk (Fig. 8.38d). A Y-shaped graft copolymer with a long anchoring chain is hardly pulled out (Fig. 8.38e). Following thermodynamic theory (equilibrium under quiescent conditions), an asymmetric copolymer is unstable at the interface. The results in Fig. 8.38 show that the external shear effect prevails over the thermodynamic effect.

Super-tough nylon is a case of the inverse-Y-type graft copolymer, which is hardly pulled out at all and stays at the interface to act as the emulsifier. It seems to be a clever and reasonable choice.

The pull-out occurs even at the very early stages of mixing in which the dispersed particles are large (∼10 μm). By continuing the mixing, the large particles shrink and the number of micelles increases. Eventually, the large particles

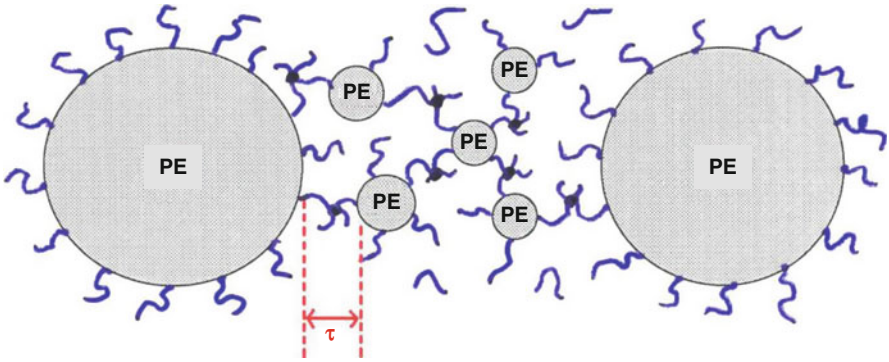


**Fig. 8.39** Bimodal particle distribution by the pull-out of in situ-formed graft copolymer

disappear, leading to a pure copolymer domain system; that is, 100 % conversion is achieved. In other words, a solvent-free synthesis of the block or graft copolymer is realized by the dry process.

If the reactive blending is stopped at an intermediate stage, the micelles and the shrunken particles coexist and a bimodal particle distribution is realized, as shown in Fig. 8.39. In the case of Fig. 8.39, PA-6 was mixed with polyethylene (PE) modified with a small amount of MAH (0.1 wt%) and glycidyl methacrylate (3–12 wt%), at a 70/30 (PA/PE) blend ratio. The bimodal system can be easily crosslinked by electron beam irradiation at a low dose level, the same as that used for neat PE (Pan et al. 2002). The crosslinked PA/PE alloy shows good heat resistance in a lead-free solder test; thus, it may be applied in making construction parts with melt-down resistance in fires, e.g., a window frame.

### 8.5.4 Pull-in of in situ-formed Copolymer

As discussed in Fig. 8.38, an in situ-formed inverse-Y shaped copolymer is hardly pulled out of the matrix. However, "pull-out into the dispersed particles" (pull-in) takes place in reactive blending by the use of an extremely long (L/D = 100, L: screw length, D: screw diameter) twin screw extruder (Sato et al. 2007). Under the intensive shear fields in the extruder, the dispersed particles can be highly deformed, as shown in Fig. 8.40. The deformation to ellipsoids and the recovery to spherical particles would be repeated in the extruder, which implies that, from the shear fields in the dispersed particles, the in situ-formed graft copolymers would pull into the dispersed particles.

The pull-in leads to a fine "salami" morphology of 20 nm occlusion, as shown in Fig. 8.40. A PA/EGMA 70/30 alloy with a fine salami morphology showed ultra-high toughness (non-break under the Izod impact test) and a non-viscoelastic tensile property: the higher deformation rate leads to a lower modulus and a larger elongation at break (Sato et al. 2007). These results suggest a potential application in energy-absorbing car parts, designed to be friendly for both pedestrian and

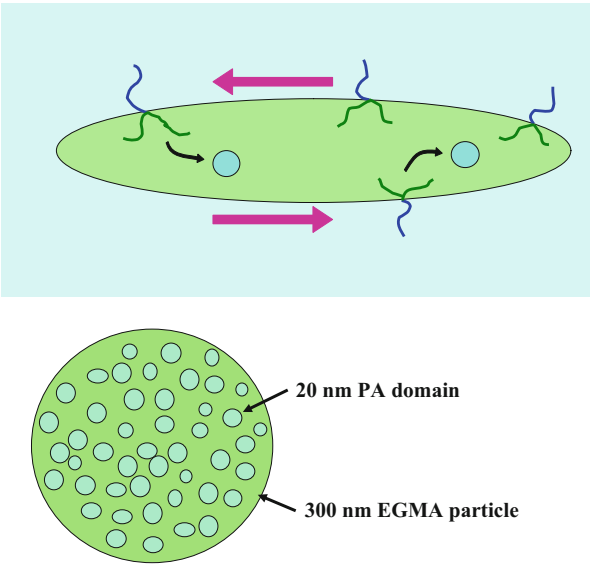


**Fig. 8.40** Pull-in of the in situ-formed inverse Y-type graft copolymer to form fine salami particle

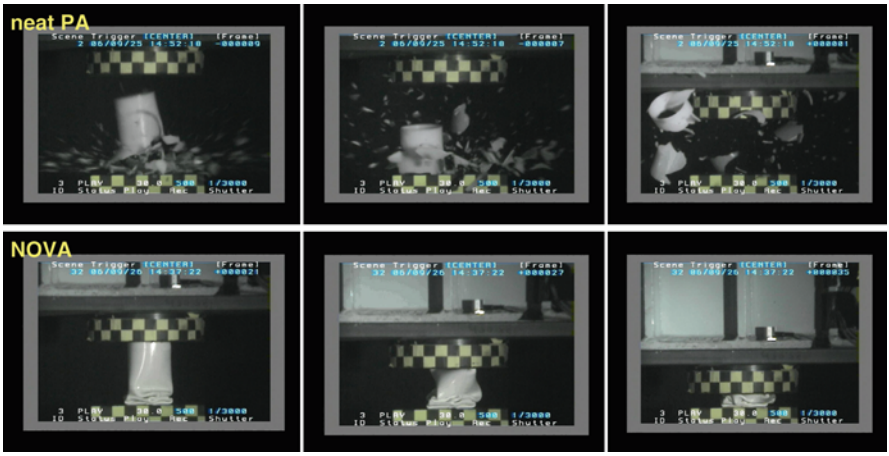


**Fig. 8.41** Video images during the falling weight impact test for neat PA (*above*) and PA/EGMA alloy (*below*)

driver. Actually, the alloy showed super-ductile behavior in a high-speed crash test. The results of a high-speed falling weight impact test are shown in Fig. 8.41 (Inoue and Kobayashi 2011). A 193 kg weight fell from a 0.5 m height (impact speed = 11.2 km/h) on a pipe sample (50 mm diameter, 150 mm height, 2 mm thick). The neat PA crashes into tiny fragments immediately after the weight hits the pipe sample. The impact condition is so severe that this typical engineering

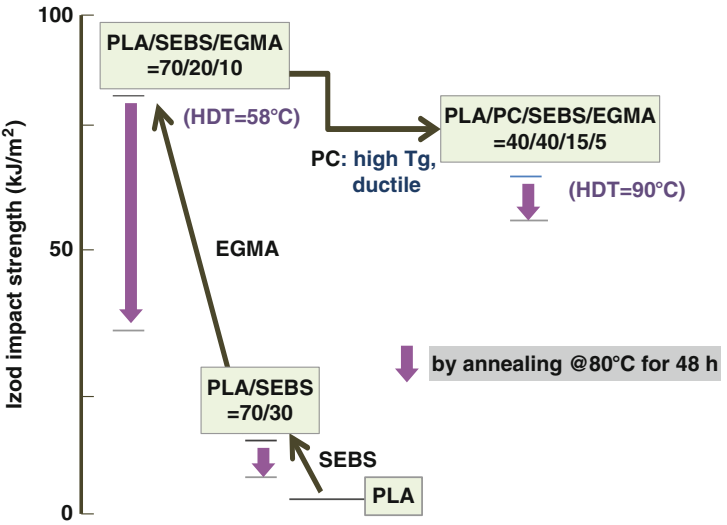


**Fig. 8.42** Improvement of toughness, heat resistance (HDT), and ageing resistance of PLA

plastic, PA, breaks in a very brittle manner. However, even for such a severe impact test, the PA/EGMA alloy never breaks, but only deforms. It looks like a beer can and a rubber hose.

### 8.5.5 Blending by Combining Many Reactions

As shown in Fig. 8.42, the toughness of poly(lactic acid) (PLA) is improved by blending a hydrogenated styrene-butadiene-styrene block copolymer (polystyrene-*b*-poly(ethylene-co-butylene)-*b*-polystyrene; SEBS). By adding EGMA as the third component, the toughness can be improved further. However, the toughness of both binary and ternary alloys decreases by annealing at 80 °C for 48 h. By adding polycarbonate (PC) as the fourth component, the heat resistance is improved; i.e., the high toughness is maintained even after the annealing (Hashima et al. 2010). The four-component alloy may be classified as an engineering plastic, as shown in Fig. 8.43.

In the TEM micrographs of Fig. 8.44, the gray region is assigned to PC and the dark region to SEBS particles in which the microdomain structure of the block copolymer is seen. SEBS particles are covered by a thin layer of EGMA. The coupling reaction between PLA and EGMA may lead to a fine dispersion of SEBS-core/EGMA-shell particles. The right micrograph is a magnified one. A gray boundary is seen between the elongated PC particles and the PLA matrix. The boundary is assigned to a multi-block or random copolymer formed by an exchange reaction between PC and PLA. The copolymer is expected to enhance the interfacial adhesive strength.

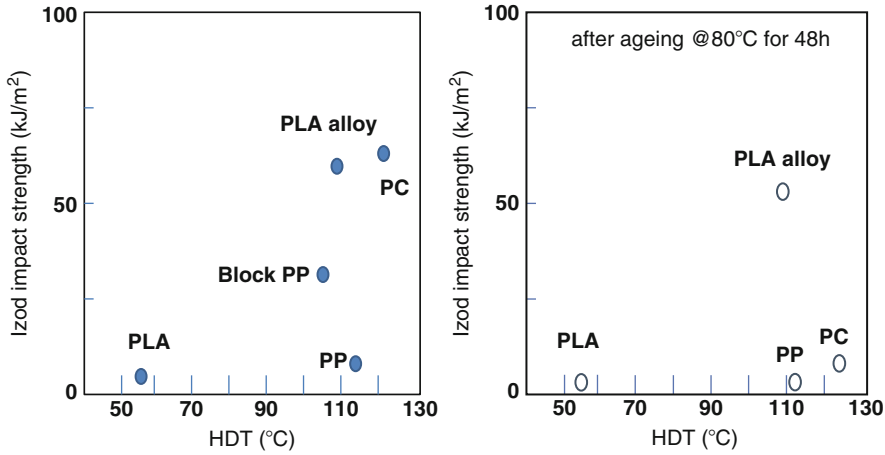


**Fig. 8.43** PLA alloy on impact strength-HDT map, as compared with other plastics

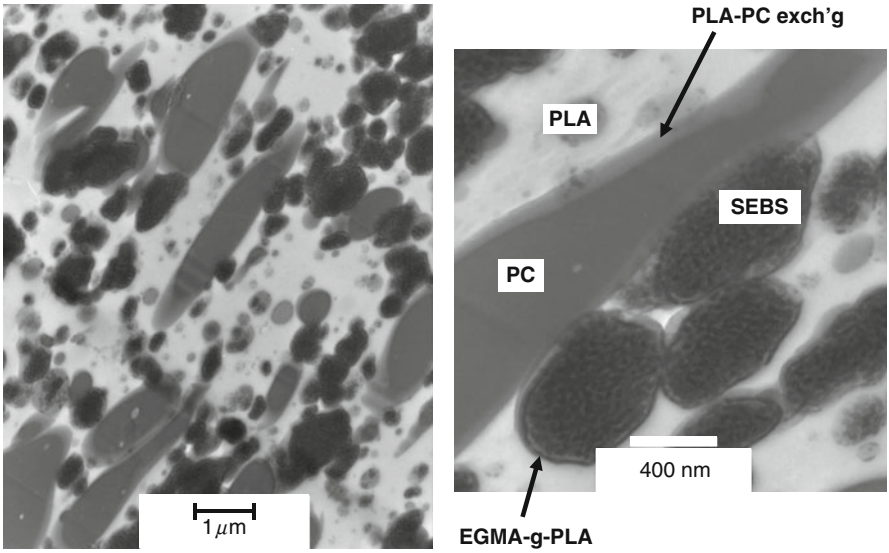


**Fig. 8.44** TEM of four component PLA alloy

Thus, the morphology of the four-component alloy seems to be generated by combining two reactions: the coupling reaction between EGMA and PLA and the exchange reaction between PC and PLA.

A high-performance PP/PLA alloy is successfully developed by reactive blending with the aid of EGMA and organic peroxide (dicumyl peroxide, DCP),

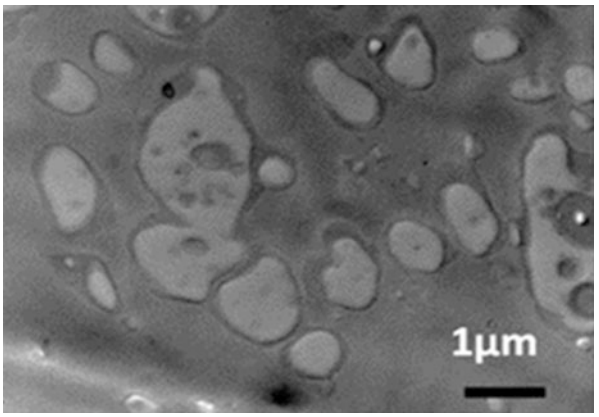


**Fig. 8.45** TEM of PLA/PP alloy

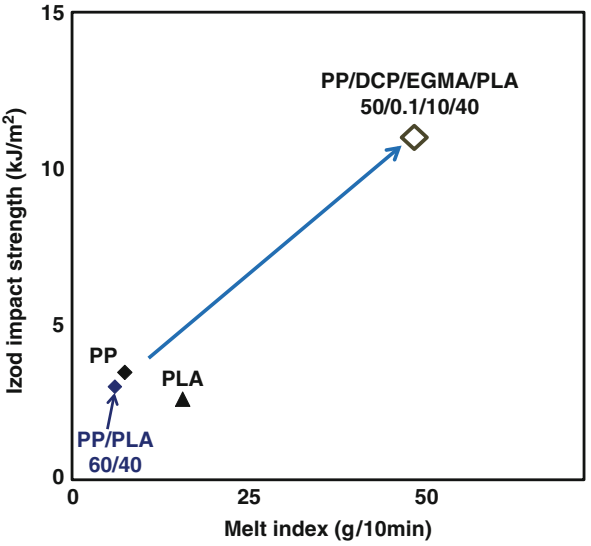


**Fig. 8.46** Impact strength and fluidity of PLA/PP alloy

e.g., PP/DCP/EGMA/PLA = 50/0.1/10/40 (Ito et al. 2012). As shown in Fig. 8.45, PLA particles are coated with EGMA shell and dispersed in a PLA matrix. The rubber (EGMA) shell seems to help the cold drawing of the brittle occlusion (PLA) in the ductile matrix (PP) (Angola et al. 1988). It showed high Izod impact strength, large elongation at break (75 %), and nice fluidity (Fig. 8.46). The three reactions involved in this reactive blending, (1) coupling between the epoxide of EGMA and the carboxyl acid and/or hydroxyl chain ends of PLA, (2) chain scission of PP, and (3) radical grafting of PP onto EGMA, may generate a desirable morphology of fine particles of PLA-core/EGMA-shell, dispersed in a PP matrix of low viscosity (see Fig. 8.47).

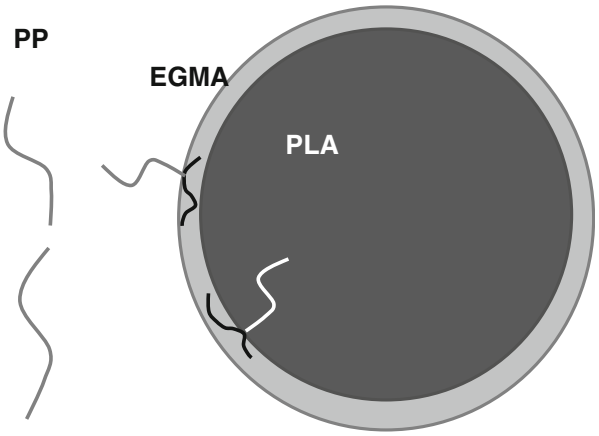


**Fig. 8.47** Chain scission of PP, PP-EGMA radical grafting, and EGMA-PLA coupling

### 8.5.6 Blending with the aid of Reactive Plasticizer

It was quite difficult to develop a high-performance PP/PC blend. The difficulty is caused by the big differences in melt viscosity (the viscosity of PC is two decades higher than that of PP) and polarity (PP: non-polar vs. PC: polar). A new approach has been presented that uses a reactive plasticizer which is preferentially soluble with PC and polymerizable by organic peroxide (Matsumoto et al. 2012). As plasticizers, diallyl phthalate (DAP) and triallyl cyanurate (TAC) are used. For example, by adding 20 wt% of DAP, the melt viscosity of PC decreases to the same level of neat PP. By the reactive extrusion of PP/PC/plasticizer/dicumyl peroxide (e.g., 80/14/6/0.12 wt. ratio), a reaction-induced phase decomposition takes place in the dispersed PC particles to develop a regularly phase-separated nanostructure, and the graft copolymer of PP and polymerized plasticizer seems to be generated in situ at the interface. The extruded blend shows an excellent ductile behavior with ca. 500 %-elongation at break. TAC is shown to be more effective at elevating the heat resistance than DAP.

## 8.6 Concluding Remarks

Here, three important phenomena to control the phase separation morphology were explained: the phase diagram and the phase separation in a shear flow field, reaction-induced phase separation, and reactive blending.

Information about the phase diagram and the phase separation in the shear flow field is very important in polymer processing. For instance, it is important to know how the miscibility and the phase diagram change in a shear flow field. As shown in this chapter, the miscible area might extend by the shear flow, and there might be a case in which a two-phase region becomes a one-phase region. After the cessation of the shear flow, the miscible area reduces and the phase separation from the one-phase state might take place by spinodal decomposition. Control of the

phase-separated morphology using such a phenomenon must exist in other systems. Moreover, it may be that the physical properties are improved by increasing the adhesion between both separated phases due to the partial dissolution even if both polymers do not mix completely.

Reaction-induced phase separation is a very useful method because of a peculiar morphology in which the major component forms the domain and the minor component the matrix (occasionally a co-continuous morphology is formed). The utility value of this morphology is high. Because there are not very many miscible polymer blends, the method of controlling the morphology by using the phase separation from the one-phase state which is obtained by using the low molecular weight one as one component of polymer blend is useful. Therefore, another effect may be assumed to induce the phase separation and the unique morphology in RIPS. Regarding the change of physical properties by polymerization, it is known that volume shrinkage occurs in the process of polymerization from monomers to polymer. Considering that the polymerized component is sure to form domains in RIPS, this volume shrinkage is assumed to induce the unique morphology. Therefore, the shrinkage stress during polymerization may be assumed to affect the formation mechanism and also bring the differential in the coarsening mechanism.

Regarding the reactive blends, control of the molecules in the interfacial region is important, because they affect the morphology and the properties. The role of the in situ-formed copolymers is related to many phenomena. Therefore, the molecular design of the copolymer, including the type of copolymer, functional group, position of functional group, block length, and molecular weight, is important.

The formation of a phase separation morphology with crystallization is also important, though it was not described in this chapter.

The control of the phase separation morphology is just a key technology in polymer blends. In order to achieve good performance of the materials, it is important to handle the processing-morphology-properties relationship.

## 8.7 Cross-References


- ▶ Interphase and Compatibilization by Addition of a Compatibilizer
- ▶ Reactive Compatibilization
- ▶ Thermodynamics of Polymer Blends


## Notation and Abbreviations

### Notation

$d_s$ Spatial dimensionality
$G_M$ Free energy of mixing
$q$ Magnitude of scattering vector
$R$ Gas constant

$r$ Number of segments in polymer chain
$S$ Spreading coefficient
$T_g$ Glass transition temperature
$T_m$ Melting temperature of crystal
$T_s$ Spinodal temperature
$V$ Volume
$\Gamma_{i/j}$ Interfacial tension between $i$ and $j$
$\dot{\gamma}$ Shear rate
$\theta$ scattering angle
$\Lambda_m$ Periodic distance
$\lambda$ Wavelength of light in the medium
$\tau$ Surface-to-surface interparticle distance
$\tau_{\xi}$ Characteristic relaxation time
$\phi_i$ Volume fraction of component $i$
$\chi_{12}$ Binary interaction parameter

## Abbreviations

**ABS** Acrylonitrile-butadiene-styrene resin
**AIBN** α,α′-azobis(isobutyronitrile)
**cPC** PC copolymer
**c-RIPS** Curing reaction-induced phase separation
**DAP** Diallyl phthalate
**DCP** Dicumyl peroxide
**EGMA** Poly(ethylene-*co*-glycidyl methacrylate)
**EPR** Ethylene-propylene rubber
**EVAc** Poly(ethylene-*co*-vinyl acetate)
**LCST** Lower critical solution temperature
**LS** Light scattering
**MAH** Maleic anhydride
**MMA** Methyl methacrylate
**NG** Nucleation and growth
**OM** Optical microscope
**PA4,6** Polyamide (nylon) 4,6
**PA-6** Polyamide (nylon) 6
**PBT** Poly(butylene terephthalate)
**PC** Bisphenol-A polycarbonate
**PE** Polyethylene
**PES** Poly(ether sulfone)
**PLA** Poly(lactic acid)
**PMMA** Poly(methyl methacrylate)
**PP** polypropylene
**PPE** Poly(phenylene ether)

**PVME** Poly(vinyl methyl ether)
**PPS** Poly(phenylene sulfide)
**p-RIPS** Polymerization reaction-induced phase separation
**PS** Polystyrene
**RIPS** Reaction-induced phase separation
**SAN** Poly(styrene-*co*-acrylonitrile)
**SD** Spinodal decomposition
**SEBS** Hydrogenated styrene-butadiene-styrene copolymer
**TAC** Triallyl cyanurate
**TEM** Transmission electron microscope
**UCST** Upper critical solution temperature

## References

J.-B. An, T. Ougizawa, T. Inoue, Y. Ishii, T. Yoshizaki, in *16th Polymer Processing Society, Abstract*. 2001, p. 21
J.-B. An, T. Suzuki, T. Ougizawa, T. Inoue, K. Mitamura, K. Kawanishi, J. Macromol. Sci. Phys. **B41**(407) (2002)
J.C. Angola, Y. Fujita, T. Sakai, T. Inoue, J. Polym. Sci. Phys. **26**, 807 (1988)
W. Baker, S. Scott, G.H. Hu (eds.), *Reactive Polymer Blending* (Hanser, Munich, 2001)
D. Beysens, M.J. Gbadamassi, Phys. Lett. (Paris) **40**, L565 (1979)
D. Beysens, F.J. Perrot, Phys. Lett. (Paris) **45**, L31 (1984)
K. Binder, D. Stauffer, Phys. Rev. Lett. **33**, 1006 (1973)
C.B. Bucknall, *Toughened Plastics* (Applied Science, London, 1977)
J.W. Cahn, J. Chem. Phys. **42**, 93 (1965)
J.W. Cahn, Trans. Met. Soc. AIME **242**, 166 (1968)
P. Charoensirisomboon, T. Chiba, S.I. Solomko, T. Inoue, Polymer **40**, 6803 (1999)
P. Charoensirisomboon, T. Inoue, M. Weber, Polymer **41**, 4483 (2000)
W. Chen, S. Kobayashi, T. Inoue, T. Ohnaga, T. Ougizawa, Polymer **35**, 4015 (1994)
A.Y. Coran, R. Patel, Rubber Chem. Technol. **56**, 1045 (1983)
B.D. Favis, J.M. Willis, J. Polym. Sci.: Polym. Phys. **28**, 2259 (1990)
J. Fernandez, J.S. Higgins, R. Horst, B. Wolf, Polymer **36**, 149 (1995)
D.J. Flory, *Principles of Polymer Chemistry* (Cornell University Press, Ithaca, 1953)
M. Furuta, Y. Koyama, T. Inoue, e-J. Soft Mater. **3**, 49 (2007)
G.M. Hanafy, S.A. Madbouly, T. Ougizawa, T. Inoue, Polymer **45**, 6879 (2004)
K. Hashima, K. Usui, L. Fu, T. Inoue, K. Fujimoto, K. Segawa, T. Abe, H. Kimura, Polym. Eng. Sci. **48**, 1207 (2008)
K. Hashima, S. Nishitsuji, T. Inoue, Polymer **51**, 3934 (2010)
E. Helfand, G.H. Fredrickson, Phys. Rev. Lett. **62**, 2468 (1989)
I.A. Hindawi, J.S. Higgins, R.A. Weiss, Polymer **33**, 2522 (1992)
J. Ibuki, P. Charoensirisomboon, T. Chiba, T. Ougizawa, T. Inoue, M. Weber, E. Koch, Polymer **40**, 647 (1999)
F. Ide, A. Hasegawa, J. Appl. Polym. Sci. **18**, 963 (1974)
T. Inoue, Prog. Polym. Sci. **20**, 119 (1995)
T. Inoue, J. Jpn. Soc. Polym. Process. **8**, 24 (1996)
T. Inoue, S. Kobayashi, Recent Res. Devel. Polym. Sci. **11**, 1 (2011)
I. Ito, M. Furuta, S. Nishituji, T. Inoue, in *28th Polymer Process Society*, Pattaya, Thailand, Dec 13 2012
H.W. Kammer, C. Kummerloewe, J. Kressler, J.P. Melior, Polymer **32**, 1488 (1991)

J. Katsaros, M. Malone, H. Winter, Polym. Eng. Sci. **29**, 1434 (1989)
T. Kojima, T. Ohnaga, T. Inoue, Polymer **36**, 2197 (1995)
F.B.C. Larbi, M.F. Malone, H.H. Winter, J.L. Halary, M.H. Leviet, L. Monnerie, Macromolecules **21**, 3534 (1988)
H. Li, Y. Yang, R. Fujitsuka, T. Ougizawa, T. Inoue, Polymer **40**, 927 (1999)
J. Lyngaae-Jorgensenn, K. Sondegaard, Polym. Eng. Sci. **27**, 351 (1987)
S.A. Madbouly, M. Ohmomo, T. Ougizawa, T. Inoue, Polymer **40**, 1465 (1999a)
S.A. Madbouly, T. Chiba, T. Ougizawa, T. Inoue, J. Macromol. Sci. Phys. B **38**, 79 (1999b)
S.A. Madbouly, T. Chiba, T. Ougizawa, T. Inoue, Polymer **42**, 1743 (2001)
L.T. Manzione, J.K. Gilliham, C.A. Mcpherson, J. Appl. Polym. Sci. **26**, 889 (1981)
K. Matsumoto, M. Nagai, K. Hamakawa, S. Nishitsuji, T. Inoue, J. Appl. Polym. Sci.(2012). doi:10.1002/App.38764
K. Mazich, S.H. Carr, J. Appl. Phys. **54**, 5511 (1983)
A.I. Nakatani, H. Kim, Y. Takahashi, Y. Matsushita, A. Takano, B.J. Bauer, C.C. Han, J. Chem. Phys. **93**, 795 (1990)
M. Okada, K. Fujimoto, T. Nose, Macromolecules **28**, 1795 (1995)
M. Okamoto, T. Inoue, Polym. Eng. Sci. **33**, 176 (1993)
M. Okamoto, K. Shiomi, T. Inoue, Polymer **36**, 87 (1995)
S. Ono, H. Isago, T. Ougizawa, Polym. Prep. Jpn **57**, 3122 (2008)
A. Onuki, K. Kawasaki, Ann. Phys. (N.Y.) **121**, 456 (1979a)
A. Onuki, K. Kawasaki, Phys. Lett. **72**, 233 (1979b)
A. Onuki, K. Yamazaki, K. Kawasaki, Ann. Phys. (N.Y.) **131**, 217 (1981)
A. Onuki, in *Taniguchi Conference on Polymer Research by Neutron Scattering*, Kyoto, Japan, Nov 1989
L. Pan, T. Inoue, H. Hayami, S. Nishikawa, Polymer **43**, 337 (2002)
L. Park, J.W. Barlow, D.R. Paul, J. Polym. Sci., Phys. Ed. **30**, 1021 (1992)
D. Sato, Y. Kadowaki, J. Ishibashi, S. Kobayashi, T. Inoue, e-J. Soft Mater. **3**, 9 (2007)
T. Takebe, R. Sawaoka, T. Hashimoto, J. Chem. Phys. **91**, 4369 (1989)
L.A. Utracki, Polym. Eng. Sci **22**, 1166 (1982)
J.J. van Aartsen, Eur. Polym. J. **6**, 919 (1970)
S. Visconti, R.H. Marchessault, Macromolecules **7**, 913 (1974)
R. Wu, M.T. Shaw, R.A. Weiss, Polym. Mater. Sci. Eng. **65**, 263 (1991)
K. Yamanaka, T. Inoue, Polymer **30**, 662 (1989)
K. Yamanaka, T. Inoue, J. Mater. Sci. **25**, 241 (1990)
K. Yamanaka, Y. Takagi, T. Inoue, Polymer, **30**, 1839 (1989)